©Saxe-Coburg Publications, 2010.
Developments and Applications in
Computational Structures Technology
B.H.V. Topping, J.M. Adam, F.J. Pallarés
R. Bru and M.L. Romero, (Editors)
Saxe-Coburg Publications, Stirlingshire, Scotland, 888-898

Chapter ?

A Modern and Compact Way to Formulate Classical and Advanced Beam Theories

E. Carrera[1], G. Giunta[2] and M. Petrolo[1,3]
[1]Department of Aeronautic and Space Engineering
Politecnico di Torino, Italy
[2]Department of Advanced Materials and Structures, Centre de
Recherche Public Henri Tudor, Luxembourg-Kirchberg, Luxembourg
[3]Institut Jean Le Rond d'Alembert, UMR7190 CNRS, Paris06, France

Abstract

A unified formulation for refined beam theories is presented. The Carrera unified formulation, CUF, is used to implement any-order beam models. The order of the formulation, N, is considered as a free parameter of the analysis. N-Order Taylor type expansions are employed to define the displacement components above the cross-section. Closed and weak form formulations are obtained. Compact and thin-walled beams (rectangular, annular, airfoil-shaped, C-shaped, bridge-like) are analyzed under different loading conditions (distributed and point loads, bending and torsional) and using different material properties (isotropic and functionally graded materials (FGM)). Free vibration analyses are conducted as well. It has been mainly concluded that higher order beam theories correctly are able to detect the mechanical behavior of short, thin-walled , and FGM made structures. CUF has offered a flexible tool easily to implement any-order beam theory independently of the considered structural problem.

Keywords: refined beam theories, finite elements, unified formulation, shell capabilities, variational statement, thin walled sections.

1 Introduction

Most known theories pertaining to the analysis of structures are due to the intuition of some structural analysis pioneers. Leonardo Da Vinci gave one of the first contributions to the theory of beam structures [1]. He correctly established all the features of the displacement field of a beam, hypothesizing a linear distribution of the strain on the cross-section. Some other well-known contributions are those by Euler [2], Bernoulli [3], Cauchy [4], Poisson [5], Kirchhoff [6], De Saint Venant [7], Timoshenko [8,9], Love [10], Reissner [11], Mindlin [12], and Vlasov [13], among others. In most cases, these 'axiomatic' intuitions led to a simplified kinematics of the true

three-dimensional deformation state of the considered structure: the section remains plane, the section/thickness deformation can be discarded, shear strains are negligible, *etc.*

Beam models are the reference technique in many applications. They are advantageous in the analysis of slender bodies, such as airplane wings, helicopter blades, bridges, frames, *etc.* The relevance of a beam theory increases to a great extent if higher-order models are developed to which plate/shell capabilities can be assigned, such as those in [14] and [15]. Like in plate and shell theories [16–21] refined beam theories can be developed according to the following two approaches:

1. the axiomatic hypothesis method;
2. the asymptotic expansion method.

Both methods permit a three-dimensional problem to be reduced to a one-dimensional one, that is, a generic variable (displacement, stress or strain component) f is expressed in terms of one or more M additional variables f_τ ($\tau = 1, M$) which are defined at an assigned point on the beam section (usually in correspondence to the beam axis). This expansion is constructed by introducing the base functions $F_\tau(x, z)$, which are defined over the beam section, as expressed by the following formula:

$$f(x, y, z) = F_\tau(x, z) f_\tau(y), \quad \tau = 1, 2, ..., M \tag{1}$$

where x and z are the cross-section coordinates, y is the beam axis coordinate and M indicates the number of terms in the expansion. If the three displacement components are considered, a possible explicit form of Equation (1) is:

$$\begin{aligned} u_x &= u_{x_1} + x\, u_{x_2} + z\, u_{x_3} \\ u_y &= u_{y_1} + x\, u_{y_2} + z\, u_{y_3} \\ u_z &= u_{z_1} + x\, u_{z_2} + z\, u_{z_3} \end{aligned} \tag{2}$$

where u_x, u_y, and u_z are the displacement components which are defined using 9 variables (u_{x_1}, u_{x_2}, ..., u_{z_3}).

In the first method, the so-called *axiomatic* method, the expression in Equation (2) is the result of an intuition of some eminent scientists. This method has permitted one-dimensional models to be developed for beams made of isotropic materials, which are known as Euler-Bernoulli's and Timoshenko's theories. The former does not account for the transverse shear effects on the cross-section deformations. The latter provides a model which foresees a constant shear deformation distribution on the cross-section. Both models yield better results for slender beams than for short beams. Refined theories can be derived assuming more sophisticated kinematics models. Excellent works concerning the development of refined beam models by means of the axiomatic approach are those by Kapania and Raciti [22, 23], Librescu and Song [24], Banerjee and Williams [26], Song and Waas [25].

In the second method, the so-called *asymptotic* method, a suitable kinematics model for a given structural problem is obtained by investigating the role played by the various variables f_τ in terms of a perturbation parameter (usually a geometrical one, such

as the span-to-height ratio for beams). The three-dimensional problem is thus reduced to a one-dimensional model by exploiting an asymptotic series of a characteristic parameter. The asymptotic approach furnishes 'consistent' approximations. This means that all the retained terms are those which have the same order of magnitude as the introduced perturbation parameter when the latter vanishes. Important contributions to the beam modelings by means of the asymptotic approach are those by Volovoi *et al.* [27], Volovoi and Hodges [28], Popescu and Hodges [29], Yu *et al.* [30], Yu and Hodges [31, 32].

This work is embedded in the framework of the Carrera Unified Formulation for beam [15, 38–43], plate and shell [20, 21, 33–37] structures. This approach was introduced by the first author during the last decade and formulates governing equations, in both strong and weak forms, in terms of a few 'fundamental nuclei' whose form does not depend on either the order of the introduced approximations or on the choices made for the base functions in the thickness direction (for plates/shells) or over the section (for beams). The present work deals with several structural problems by means of higher-order beam theories. Analytical and finite element approaches are taken into account. Structures having different geometries (compact and thin-walled) and loadings (bending and torsion) are analyzed. Isotropic and FGM materials are accounted for. The results are compared with those retrieved from the open literature and with those obtained through shell and solid models. This chapter is organized as follows. The modeling approach is described in Sections 2 and 3. The results and their discussion are given in Section 4. The main conclusions and the outlooks are drawn in Section 5.

2 Considered Beam Theories

Classical and higher-order theories are considered in this work. The adopted coordinate frame is presented in Figure 1. The beam boundaries over y are $0 \leq y \leq L$. The

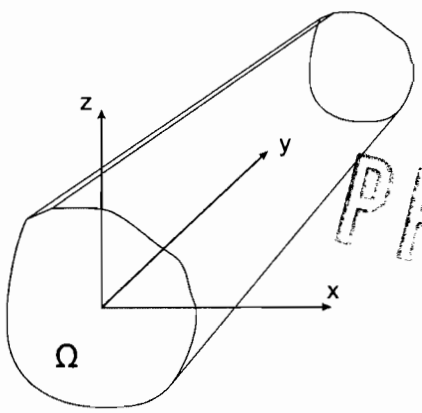

Figure 1: Coordinate frame of the beam model

displacement vector is:

$$\mathbf{u}(x,y,z) = \left\{ \begin{array}{ccc} u_x & u_y & u_z \end{array} \right\}^T \tag{3}$$

The superscript "T" represents the transposition operator. Stress, $\boldsymbol{\sigma}$, and strain, ϵ, components are grouped as follows:

$$\begin{array}{l} \boldsymbol{\sigma}_p = \left\{ \begin{array}{ccc} \sigma_{zz} & \sigma_{xx} & \sigma_{zx} \end{array} \right\}^T, \quad \boldsymbol{\epsilon}_p = \left\{ \begin{array}{ccc} \epsilon_{zz} & \epsilon_{xx} & \epsilon_{zx} \end{array} \right\}^T \\ \boldsymbol{\sigma}_n = \left\{ \begin{array}{ccc} \sigma_{zy} & \sigma_{xy} & \sigma_{yy} \end{array} \right\}^T, \quad \boldsymbol{\epsilon}_n = \left\{ \begin{array}{ccc} \epsilon_{zy} & \epsilon_{xy} & \epsilon_{yy} \end{array} \right\}^T \end{array} \tag{4}$$

The subscript "n" stands for terms lying on the cross-section, while "p" stands for terms lying on planes which are orthogonal to Ω. Linear strain-displacement relations are used:

$$\begin{array}{l} \boldsymbol{\epsilon}_p = \boldsymbol{D}_p \mathbf{u} \\ \boldsymbol{\epsilon}_n = \boldsymbol{D}_n \mathbf{u} = (\boldsymbol{D}_{n\Omega} + \boldsymbol{D}_{ny}) \mathbf{u} \end{array} \tag{5}$$

With:

$$\boldsymbol{D}_p = \begin{bmatrix} 0 & 0 & \frac{\partial}{\partial z} \\ \frac{\partial}{\partial x} & 0 & 0 \\ \frac{\partial}{\partial z} & 0 & \frac{\partial}{\partial x} \end{bmatrix}, \quad \boldsymbol{D}_{n\Omega} = \begin{bmatrix} 0 & 0 & 0 \\ 0 & \frac{\partial}{\partial x} & 0 \\ 0 & \frac{\partial}{\partial z} & 0 \end{bmatrix}, \quad \boldsymbol{D}_{ny} = \begin{bmatrix} 0 & \frac{\partial}{\partial y} & 0 \\ \frac{\partial}{\partial y} & 0 & 0 \\ 0 & 0 & \frac{\partial}{\partial y} \end{bmatrix} \tag{6}$$

Under the hypothesis of isotropic linear elastic FGMs, the generalised Hooke's law holds:

$$\boldsymbol{\sigma} = \boldsymbol{C}(x,z)\epsilon \tag{7}$$

According to Equations 4, the previous equation becomes:

$$\begin{array}{l} \boldsymbol{\sigma}_p = \tilde{\boldsymbol{C}}(x,z)_{pp}\boldsymbol{\epsilon}_p + \tilde{\boldsymbol{C}}(x,z)_{pn}\boldsymbol{\epsilon}_n \\ \boldsymbol{\sigma}_n = \tilde{\boldsymbol{C}}(x,z)_{np}\boldsymbol{\epsilon}_p + \tilde{\boldsymbol{C}}(x,z)_{nn}\boldsymbol{\epsilon}_n \end{array} \tag{8}$$

As far as the material properties are concerned, Young's modulus, E, is supposed to vary with respect to x and z coordinates according to the following exponential law:

$$E(x,z) = E_0 e^{(\alpha_1 x + \beta_1)} e^{(\alpha_2 z + \beta_2)} \tag{9}$$

Poisson's ratio, ν, is considered constant. Matrices $\mathbf{C}_{pp}$, $\mathbf{C}_{pn}$, $\mathbf{C}_{np}$ and $\mathbf{C}_{nn}$ in Equations (8) are:

$$\tilde{\boldsymbol{C}}_{pp} = \begin{bmatrix} \tilde{C}_{11} & \tilde{C}_{12} & 0 \\ \tilde{C}_{12} & \tilde{C}_{22} & 0 \\ 0 & 0 & \tilde{C}_{66} \end{bmatrix} e^{(\alpha_1 x + \alpha_2 z)} \quad \tilde{\boldsymbol{C}}_{nn} = \begin{bmatrix} \tilde{C}_{55} & 0 & 0 \\ 0 & \tilde{C}_{44} & 0 \\ 0 & 0 & \tilde{C}_{33} \end{bmatrix} e^{(\alpha_1 x + \alpha_2 z)}$$

$$\tilde{\boldsymbol{C}}_{pn} = \tilde{\boldsymbol{C}}_{np}^T = \begin{bmatrix} 0 & 0 & \tilde{C}_{13} \\ 0 & 0 & \tilde{C}_{23} \\ 0 & 0 & 0 \end{bmatrix} e^{(\alpha_1 x + \alpha_2 z)} \tag{10}$$

where the constant stiffness coefficients $\tilde{C}_{ij}$ are:

$$\begin{aligned}
\tilde{C}_{11} = \tilde{C}_{22} = \tilde{C}_{33} &= \frac{1-\nu}{(1+\nu)(1-2\nu)} E_0 e^{(\beta_1+\beta_2)} \\
\tilde{C}_{12} = \tilde{C}_{13} = \tilde{C}_{23} &= \frac{\nu}{(1+\nu)(1-2\nu)} E_0 e^{(\beta_1+\beta_2)} \\
\tilde{C}_{44} = \tilde{C}_{55} = \tilde{C}_{66} &= \frac{1}{2(1+\nu)} E_0 e^{(\beta_1+\beta_2)}
\end{aligned} \tag{11}$$

2.1 Classical Theories: Euler-Bernoulli's and Timoshenko's Beam Models

Classical beam theories are those by Euler-Bernoulli (EBBM) and Timoshenko (TBM). These models are based on first-order approximation of the kinematic field. EBBM was formulated to describe the bending mechanics, it does not account for the transverse shear effects. The kinematic field upon the cross-section of the EBBM theory is given by:

$$\begin{aligned}
u_x &= u_{x_1} \\
u_y &= u_{y_1} - x\, u_{x_1,y} - z\, u_{z_1,y} \\
u_z &= u_{z_1}
\end{aligned} \tag{12}$$

TBM foresees constant stress and strain shear distributions. In this case the displacement field becomes:

$$\begin{aligned}
u_x &= u_{x_1} \\
u_y &= u_{y_1} + x\, u_{y_2} + z\, u_{y_3} \\
u_z &= u_{z_1}
\end{aligned} \tag{13}$$

EBBM and TBM require the correction of the material coefficients to contrast Poisson's locking.

2.2 Refined Theories via Unified Formulation

In the framework of the Carrera unified formulation (CUF) [15, 20, 21, 38, 39, 41], the displacement field is assumed as an expansion in terms of generic functions, F_τ:

$$\mathbf{u} = F_\tau \mathbf{u}_\tau, \qquad \tau = 1, 2, ..., M \tag{14}$$

where F_τ are functions of the coordinates x and z on the cross-section. $\mathbf{u}_\tau$ is the displacement vector and M stands for the number of terms of the expansion. According to the Einstein notation, the repeated subscript τ indicates summation. Equation (14) consists of a Maclaurin expansion that uses the 2D polynomials $x^i\, z^j$ as base, where i and j are positive integers. Table 1 presents M and F_τ as functions of N. For example, the second-order displacement field is:

$$\begin{aligned}
u_x &= u_{x_1} + x\, u_{x_2} + z\, u_{x_3} + x^2\, u_{x_4} + xz\, u_{x_5} + z^2\, u_{x_6} \\
u_y &= u_{y_1} + x\, u_{y_2} + z\, u_{z_3} + x^2\, u_{z_4} + xz\, u_{z_5} + z^2\, u_{z_6} \\
u_z &= u_{z_1} + x\, u_{z_2} + z\, u_{z_3} + x^2\, u_{z_4} + xz\, u_{z_5} + z^2\, u_{z_6}
\end{aligned} \tag{15}$$

N	M	F_τ
0	1	$F_1 = 1$
1	3	$F_2 = x \; F_3 = z$
2	6	$F_4 = x^2 \; F_5 = xz \; F_6 = z^2$
3	10	$F_7 = x^3 \; F_8 = x^2 z \; F_9 = xz^2 \; F_{10} = z^3$
...	...	...
N	$\frac{(N+1)(N+2)}{2}$	$F_{\frac{N^2+N+2}{2}} = x^N \; F_{\frac{N^2+N+4}{2}} = x^{N-1}z \; \dots \; F_{\frac{N(N+3)}{2}} = xz^{N-1} \; F_{\frac{(N+1)(N+2)}{2}} = z^N$

Table 1: Maclaurin's polynomials

EBBM and TBM can be obtained by acting on the F_τ expansion. Classical theories and first-order models require the assumption of opportunely reduced material stiffness coefficients to correct Poisson's locking (see Carrera and Brischetto [50, 51]). Unless differently specified, for classical and first-order models Poisson's locking is corrected according to Carrera and Giunta [15].

3 Governing Equations

The principle of virtual displacements (PVD) is exploited to obtain the strong and the weak forms of the governing equations in terms of displacement components.

3.1 Strong Form

The strong form of the governing differential equations and the boundary conditions are obtained by the PVD:

$$\delta L_i = \delta L_p + \delta L_l \tag{16}$$

L_i represents the strain energy. L_p and L_l stand for the work due to a surface loading, p^k, and a line loading, l^k that act on a k sub-domain. δ stands for a virtual variation.

Variation of the Strain Energy

According to the grouping of the stress and strain components in Equation (4), the virtual variation of the strain energy is considered as the sum of two contributions:

$$\delta L_i = \int_l \int_\Omega \delta \boldsymbol{\epsilon}_n^T \boldsymbol{\sigma}_n \, d\Omega \, dy + \int_l \int_\Omega \delta \boldsymbol{\epsilon}_p^T \boldsymbol{\sigma}_p \, d\Omega \, dy \tag{17}$$

The virtual variation of the strain energy in a compact vectorial form is:

$$\delta L_i = \int_l \delta \mathbf{u}_\tau^T \, \mathbf{K}^{\tau s} \, \mathbf{u}_s \, dy + \delta \mathbf{u}_\tau^T \, \mathbf{\Pi}^{\tau s} \, \mathbf{u}_s \Big|_{y=0}^{y=L} \tag{18}$$

The components of the differential matrix $\mathbf{K}^{\tau s}$ are:

$$K_{xx}^{\tau s} = J_{\tau,x s,x}^{22k} + J_{\tau,z s,z}^{66k} - J_{\tau s}^{44k} \frac{\partial^2}{\partial y^2}$$

$$K_{yy}^{\tau s} = J_{\tau,_x s,_x}^{44k} + J_{\tau,_z s,_z}^{55k} - J_{\tau s}^{33k}\frac{\partial^2}{\partial y^2}$$

$$K_{zz}^{\tau s} = J_{\tau,_z s,_z}^{11k} + J_{\tau,_x s,_x}^{66k} - J_{\tau s}^{55k}\frac{\partial^2}{\partial y^2}$$

$$K_{zx}^{\tau s} = J_{\tau,_z s,_x}^{12k} + J_{\tau,_x s,_z}^{66k} \quad K_{xz}^{\tau s} = J_{\tau,_x s,_z}^{12k} + J_{\tau,_z s,_x}^{66k}$$

$$K_{zy}^{\tau s} = \left(J_{\tau,_z s}^{13k} - J_{\tau s,_z}^{55k}\right)\frac{\partial}{\partial y} \quad K_{yz}^{\tau s} = -\left(J_{\tau s,_z}^{13k} - J_{\tau,_z s}^{55k}\right)\frac{\partial}{\partial y}$$

$$K_{xy}^{\tau s} = \left(J_{\tau,_x s}^{23k} - J_{\tau s,_x}^{44k}\right)\frac{\partial}{\partial y} \quad K_{yx}^{\tau s} = -\left(J_{\tau s,_x}^{23k} - J_{\tau,_x s}^{44k}\right)\frac{\partial}{\partial y} \tag{19}$$

The generic terms $J_{\tau,_\phi s,_\xi}^{ggk}$, $J_{\tau s}^{ggk}$, $J_{\tau,_\phi s}^{ghk}$ and $J_{\tau s,_\phi}^{ghk}$ are the cross-section inertial momenta of a k sub-domain that account for the material gradation:

$$\begin{aligned} J_{\tau,_\phi s,_\xi}^{ggk} &= \int_{\Omega^k} C_{gg}^k e^{(\alpha_1 x+\alpha_2 z)} F_{\tau,_\phi} F_{s,_\xi}\, d\Omega \quad J_{\tau s}^{ggk} = \int_{\Omega^k} C_{gg}^k e^{(\alpha_1 x+\alpha_2 z)} F_\tau F_s\, d\Omega \\ J_{\tau,_\phi s}^{ghk} &= \int_{\Omega^k} C_{gh}^k e^{(\alpha_1 x+\alpha_2 z)} F_{\tau,_\phi} F_s\, d\Omega \quad J_{\tau s,_\phi}^{ghk} = \int_{\Omega^k} C_{gh}^k e^{(\alpha_1 x+\alpha_2 z)} F_\tau F_{s,_\phi}\, d\Omega \end{aligned} \tag{20}$$

As far as the boundary conditions are concerned, the components of $\mathbf{\Pi}^{\tau s}$ are:

$$\Pi_{xx}^{\tau s} = J_{\tau s}^{44k}\frac{\partial}{\partial y}, \quad \Pi_{yy}^{\tau s} = J_{\tau s}^{33k}\frac{\partial}{\partial y}, \quad \Pi_{zz}^{\tau s} = J_{\tau s}^{55k}\frac{\partial}{\partial y},$$
$$\Pi_{zx}^{\tau s} = \Pi_{xz}^{\tau s} = 0,$$
$$\Pi_{zy}^{\tau s} = J_{\tau s,_z}^{55k}, \quad \Pi_{xy}^{\tau s} = J_{\tau s,_x}^{44k}, \quad \Pi_{yz}^{\tau s} = J_{\tau s,_z}^{13k} \quad \Pi_{yx}^{\tau s} = J_{\tau s,_x}^{23k} \tag{21}$$

Virtual Work of the External Loadings

The virtual work done by the external loadings is assumed to be due to a surface loading and a line loading.

The components of a surface loading are:

$$\mathbf{p}^{kT} = \left\{ \begin{array}{cccccc} p_{xx}^{k\pm} & p_{xy}^{k\pm} & p_{xz}^{k\pm} & p_{zx}^{k\pm} & p_{zy}^{k\pm} & p_{zz}^{k\pm} \end{array} \right\} \tag{22}$$

They act as shown in Figure 2. The lateral surfaces $\left\{S_\phi^{k\pm} : \phi = x, z\right\}$ of the beam are defined on the basis of the normal versor $\left\{n_\phi^{k\pm} : \phi = x, z\right\}$. A normal versor with the same orientation as the x or z axis identifies a positive lateral surface. The external virtual work due to $\mathbf{p}$ is:

$$\delta L_p = \left(\delta L_{p_{xx}^\pm}^k + \delta L_{p_{xy}^\pm}^k + \delta L_{p_{xz}^\pm}^k + \delta L_{p_{zx}^\pm}^k + \delta L_{p_{zy}^\pm}^k + \delta L_{p_{zz}^\pm}^k\right)_k \tag{23}$$

Its explicit terms are:

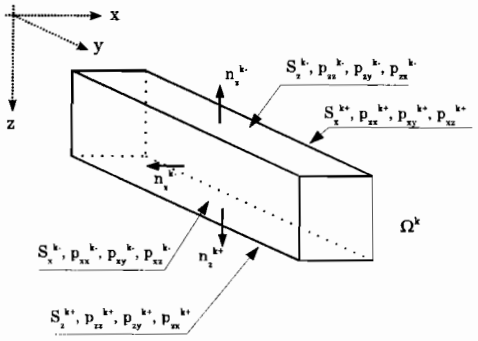

Figure 2: Components of a surface loading; lateral surfaces and normal vectors of the beam

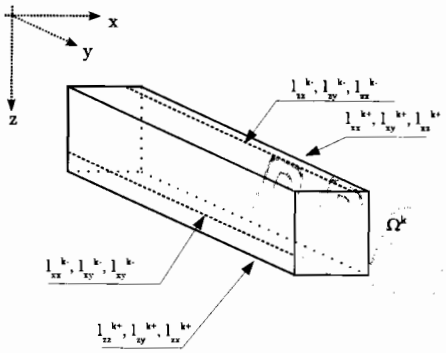

Figure 3: Components of a line loading

$$\left(\delta L^k_{p^{\pm}_{xx}},\ \delta L^k_{p^{\pm}_{zx}}\right) = \int_l \delta u_{x\tau}\left(p^{k\pm}_{xx} E^{kz^{\pm}}_{\tau},\ p^{k\pm}_{zx} E^{kx^{\pm}}_{\tau}\right)\ dy$$

$$\left(\delta L^k_{p^{\pm}_{zz}},\ \delta L^k_{p^{\pm}_{xz}}\right) = \int_l \delta u_{z\tau}\left(p^{k\pm}_{zz} E^{kx^{\pm}}_{\tau},\ p^{k\pm}_{xz} E^{kz^{\pm}}_{\tau}\right)\ dy$$

$$\left(\delta L^k_{p^{\pm}_{zy}},\ \delta L^k_{p^{\pm}_{xy}}\right) = \int_l \delta u_{y\tau}\left(p^{k\pm}_{zy} E^{kx^{\pm}}_{\tau},\ p^{k\pm}_{xy} E^{kz^{\pm}}_{\tau}\right)\ dy \qquad (24)$$

Where:

$$\left(E^{kx^+}_{\tau}, E^{kx^-}_{\tau}\right) = \int_{x^k_1}^{x^k_2} \left(F_\tau\left(z^k_2, x\right), F_\tau\left(z^k_1, x\right)\right)\ dx$$

$$\left(E^{kz^+}_{\tau}, E^{kz^-}_{\tau}\right) = \int_{z^k_1}^{z^k_2} \left(F_\tau\left(z, x^k_2\right), F_\tau\left(z, x^k_1\right)\right)\ dz \qquad (25)$$

The components of a line loading (see Figure 3) are:

$$\mathrm{l}^{kT} = \left\{\ l^{k\pm}_{xx}\quad l^{k\pm}_{xy}\quad l^{k\pm}_{xz}\quad l^{k\pm}_{zx}\quad l^{k\pm}_{zy}\quad l^{k\pm}_{zz}\ \right\} \qquad (26)$$

The external virtual work is:

$$\delta L_l = \left(\delta L^k_{l^{\pm}_{xx}} + \delta L^k_{l^{\pm}_{zz}} + \delta L^k_{l^{\pm}_{zy}} + \delta L^k_{l^{\pm}_{xy}} + \delta L^k_{l^{\pm}_{zx}} + \delta L^k_{l^{\pm}_{xz}}\right)_k \qquad (27)$$

whose terms are:

$$\left(\delta L^k_{l^{\pm}_{zz}},\ \delta L^k_{l^{\pm}_{xz}}\right) = \int_l \delta u_{z\tau}\left(l^{k\pm}_{zz} F_\tau\left(z^k_{l^{\pm}_{zz}}, x^k_{l^{\pm}_{zz}}\right),\ l^{k\pm}_{xz} F_\tau\left(z^k_{l^{\pm}_{xz}}, x^k_{l^{\pm}_{xz}}\right)\right)\ dy$$

$$\left(\delta L^k_{l^{\pm}_{xx}},\ \delta L^k_{l^{\pm}_{zx}}\right) = \int_l \delta u_{x\tau}\left(l^{k\pm}_{xx} F_\tau\left(z^k_{l^{\pm}_{xx}}, x^k_{l^{\pm}_{xx}}\right),\ l^{k\pm}_{zx} F_\tau\left(z^k_{l^{\pm}_{zx}}, x^k_{l^{\pm}_{zx}}\right)\right)\ dy$$

$$\left(\delta L^k_{l^{\pm}_{zy}},\ \delta L^k_{l^{\pm}_{xy}}\right) = \int_l \delta u_{y\tau}\left(l^{k\pm}_{zy} F_\tau\left(z^k_{l^{\pm}_{zy}}, x^k_{l^{\pm}_{zy}}\right),\ l^{k\pm}_{xy} F_\tau\left(z^k_{l^{\pm}_{xy}}, x^k_{l^{\pm}_{xy}}\right)\right)\ dy \tag{28}$$

where $\left\{\left(z^k_{l^{\pm}_{ij}}, x^k_{l^{\pm}_{ij}}\right) :\ i = z, x;\ j = z, x, y\right\}$ are the coordinates of the line loading application point above a k cross-section sub-domain.

The Fundamental Nucleus

The explicit form of the fundamental nucleus of the governing equations is obtained from Equations (19), (24) and (28):

$$\begin{aligned}
&\delta u_{x\tau}: \\
&\left(J^{12k}_{\tau,xs,z} + J^{66k}_{\tau,zs,x}\right) u_{zs} + \left(J^{22k}_{\tau,xs,x} + J^{66k}_{\tau,zs,z}\right) u_{xs} \\
&-J^{44k}_{\tau s} u_{xs,yy} + \left(J^{23k}_{\tau,xs} - J^{44k}_{\tau s,x}\right) u_{ys,y} = \\
&\left[p^{k\pm}_{xx} E^{kz^{\pm}}_{\tau} + p^{k\pm}_{zx} E^{kx^{\pm}}_{\tau} + l^{k\pm}_{xx} F_\tau\left(z^k_{l^{\pm}_{xx}}, x^k_{l^{\pm}_{xx}}\right) + l^{k\pm}_{zx} F_\tau\left(z^k_{l^{\pm}_{zx}}, x^k_{l^{\pm}_{zx}}\right)\right]_k
\end{aligned}$$

$$\begin{aligned}
&\delta u_{y\tau}: \\
&-\left(J^{13k}_{\tau s,z} - J^{55k}_{\tau,zs}\right) u_{zs,y} - \left(J^{13k}_{\tau s,x} - J^{44k}_{\tau,xs}\right) u_{xs,y} \\
&+\left(J^{44k}_{\tau,xs,x} + J^{55k}_{\tau,zs,z}\right) u_{ys} - J^{33k}_{\tau s} u_{ys,yy} = \\
&\left[p^{k\pm}_{zy} E^{kx^{\pm}}_{\tau} + p^{k\pm}_{xy} E^{kz^{\pm}}_{\tau} + l^{k\pm}_{zy} F_\tau\left(z^k_{l^{\pm}_{zy}}, x^k_{l^{\pm}_{zy}}\right) + l^{k\pm}_{xy} F_\tau\left(z^k_{l^{\pm}_{xy}}, x^k_{l^{\pm}_{xy}}\right)\right]_k
\end{aligned} \tag{29}$$

$$\begin{aligned}
&\delta u_{z\tau}: \\
&\left(J^{11k}_{\tau,zs,z} + J^{66k}_{\tau,xs,x}\right) u_{zs} - J^{55k}_{\tau s} u_{zs,yy} \\
&+\left(J^{12k}_{\tau,zs,x} + J^{66k}_{\tau,xs,z}\right) u_{xs} + \left(J^{13k}_{\tau,zs} - J^{55k}_{\tau s,z}\right) u_{ys,y} = \\
&\left[p^{k\pm}_{zz} E^{kx^{\pm}}_{\tau} + p^{k\pm}_{xz} E^{kz^{\pm}}_{\tau} + l^{k\pm}_{zz} F_\tau\left(z^k_{l^{\pm}_{zz}}, x^k_{l^{\pm}_{zz}}\right) + l^{k\pm}_{xz} F_\tau\left(z^k_{l^{\pm}_{xz}}, x^k_{l^{\pm}_{xz}}\right)\right]_k
\end{aligned}$$

The boundary conditions are:

$$\begin{aligned}
&\left[\delta u_{x\tau}\left(J^{44k}_{\tau s} u_{xs,y} + J^{44k}_{\tau s,x} u_{ys}\right)\right]_{y=0}^{y=L} = 0 \\
&\left[\delta u_{y\tau}\left(J^{13k}_{\tau s,z} u_{zs} + J^{23k}_{\tau s,x} u_{xs} + J^{33k}_{\tau s} u_{ys,y}\right)\right]_{y=0}^{y=L} = 0 \\
&\left[\delta u_{z\tau}\left(J^{55k}_{\tau s} u_{zs,y} + J^{55k}_{\tau s,z} u_{ys}\right)\right]_{y=0}^{y=L} = 0
\end{aligned} \tag{30}$$

For a fixed approximation order, the nucleus has to be expanded versus the indexes τ and s in order to obtain the governing equations and the boundary conditions that concern the desired model.

Closed Form Analytical Solution

The differential equations in Equations (29) and the related boundary conditions in Equations (30) are solved via a Navier type solution by adopting the following displacement field:

$$\begin{aligned} u_{x\tau} &= U_{x\tau} F_\tau (x,z) \sin(\alpha y) \\ u_{y\tau} &= U_{y\tau} F_\tau (x,z) \sin(\alpha y) \\ u_{z\tau} &= U_{z\tau} F_\tau (x,z) \cos(\alpha y) \end{aligned} \tag{31}$$

On the assumption that the external loadings vary towards z in the following manner:

$$\mathbf{p}^k = \left\{ \begin{array}{c} P_{xx}^{k\pm} \sin(\alpha y) \\ P_{xy}^{k\pm} \cos(\alpha y) \\ P_{xz}^{k\pm} \sin(\alpha y) \\ P_{zx}^{k\pm} \sin(\alpha y) \\ P_{zy}^{k\pm} \cos(\alpha y) \\ P_{zz}^{k\pm} \sin(\alpha y) \end{array} \right\} \quad \mathbf{l}^k = \left\{ \begin{array}{c} L_{xx}^{k\pm} \sin(\alpha y) \\ L_{xy}^{k\pm} \cos(\alpha y) \\ L_{xz}^{k\pm} \sin(\alpha y) \\ L_{zx}^{k\pm} \sin(\alpha y) \\ L_{zy}^{k\pm} \cos(\alpha y) \\ L_{zz}^{k\pm} \sin(\alpha y) \end{array} \right\} \tag{32}$$

This last assumption does not represent a loss in generality, since a generic loading can be approximated via its Fourier's series expansion (see [44,45]). The term α is:

$$\alpha = \frac{m\pi}{L} \tag{33}$$

Where m represents the half-wave number along the beam axis. $\{U_{i\tau} : i = x,y,z\}$ are the maximal amplitudes of the displacement components and $\left\{P_{i,j}^{k\pm} : i = x,z; j = x,y,z\right\}$ and $\left\{L_{i,j}^{k\pm} : i = x,z; j = x,y,z\right\}$ the maximal amplitudes of the surface and line loading, respectively. The displacement field in Equations (31) satisfies the boundary conditions, Equations (30), since:

$$\begin{aligned} u_{x\tau}(0) &= u_{x\tau}(L) = 0 \\ u_{y\tau,y}(0) &= u_{y\tau,y}(L) = 0 \\ u_{z\tau}(0) &= u_{z\tau}(L) = 0 \end{aligned} \tag{34}$$

The fundamental algebraic nucleus is obtained from Equations (29) upon substitution of Equations (31) and (32):

$$\begin{aligned} &\delta U_{x\tau} : \\ &\left(J_{\tau,xs,z}^{12k} + J_{\tau,zs,x}^{66k}\right) U_{zs} + \left(J_{\tau,xs,x}^{22k} + J_{\tau,zs,z}^{66k} + \alpha^2 J_{\tau s}^{44k}\right) U_{xs} \\ &-\alpha \left(J_{\tau,xs}^{23k} - J_{\tau s,x}^{44k}\right) U_{ys} = \left[P_{xx}^{k\pm} E_\tau^{kz\pm} + P_{zx}^{k\pm} E_\tau^{kx\pm} + L_{xx}^{k\pm} F_\tau \left(z_{l_{xx}^{\pm}}^k, x_{l_{xx}^{\pm}}^k\right)\right. \\ &\left. + L_{zx}^{k\pm} F_\tau \left(z_{l_{zx}^{\pm}}^k, x_{l_{zx}^{\pm}}^k\right)\right]_k \end{aligned}$$

$$
\begin{aligned}
&\delta U_{y\tau}: \\
&-\alpha\left(J^{13k}_{\tau,_{zs}}-J^{55k}_{\tau,_{zs}}\right)U_{zs}-\alpha\left(J^{23k}_{\tau s,_{x}}-J^{44k}_{\tau,_{xs}}\right)U_{xs} \\
&+\left(J^{44k}_{\tau,_{xs,x}}+J^{55k}_{\tau,_{zs,z}}+\alpha^2 J^{33k}_{\tau s}\right)U_{ys}= \\
&\left[P^{k\pm}_{zy}E^{kx^{\pm}}_{\tau}+P^{k\pm}_{xy}E^{kz^{\pm}}_{\tau}+L^{k\pm}_{zy}F_{\tau}\left(z^{k}_{l^{\pm}_{zy}},x^{k}_{l^{\pm}_{zy}}\right)+L^{k\pm}_{xy}F_{\tau}\left(x^{k}_{l^{\pm}_{xy}},y^{k}_{l^{\pm}_{zy}}\right)\right]_{k} \qquad (35)
\end{aligned}
$$

$$
\begin{aligned}
&\delta U_{z\tau}: \\
&\left(J^{11k}_{\tau,_{zs,z}}+J^{66k}_{\tau,_{xs,x}}+\alpha^2 J^{55k}_{\tau s}\right)U_{zs}+\left(J^{12k}_{\tau,_{zs,x}}+J^{66k}_{\tau,_{xs,z}}\right)U_{xs} \\
&-\alpha\left(J^{13k}_{\tau,_{zs}}-J^{55k}_{\tau s,_{z}}\right)U_{ys}=\left[P^{k\pm}_{zz}E^{kx^{\pm}}_{\tau}+P^{k\pm}_{xz}E^{kz^{\pm}}_{\tau}+L^{k\pm}_{zz}F_{\tau}\left(z^{k}_{l^{\pm}_{zz}},x^{k}_{l^{\pm}_{zz}}\right)\right. \\
&\left.+L^{k\pm}_{xz}F_{\tau}\left(z^{k}_{l^{\pm}_{xz}},x^{k}_{l^{\pm}_{xz}}\right)\right]_{k}
\end{aligned}
$$

For a fixed approximation order, the algebraic system has to be assembled according to the summation indices τ and s. Its solution yields the maximal displacement amplitudes. The strains are retrieved by the geometric relations, Equations (3), and the stresses via the generalized Hooke's law, Equations (8).

3.2 Weak Form

The weak form of the governing equations is obtained by means of the finite element method. The following formulation is valid only for structures made of materials with constant properties above the cross-section. The nodal displacement vector, $\mathbf{q}_{\tau i}$, is introduced:

$$
\mathbf{q}_{\tau i}=\left\{\begin{array}{ccc} q_{u_{x_{\tau i}}} & q_{u_{y_{\tau i}}} & q_{u_{z_{\tau i}}} \end{array}\right\}^{T} \qquad (36)
$$

The displacement vector becomes:

$$
\mathbf{u}_{\tau}=N_i F_{\tau}\mathbf{q}_{\tau i} \qquad (37)
$$

Where N_i are the shape functions whose expressions are not reported here for the sake of brevity, they can be found in many books, for instance in [52]. Elements with 4 nodes (B4) are herein adopted, that is, a cubic approximation along the y axis is adopted. It has to be highlighted that, while the order of the beam model is related to the expansion on the cross-section, the number of nodes per each element is related to the approximation along the longitudinal axis. These two parameters are totally free and not related to each other. An N-order beam model is therefore a theory which exploits an N-order polynomial to describe the kinematics of the cross-section. The stiffness matrix of the elements and the external loadings, which are consistent with the model, are obtained via the principle of virtual displacements:

$$
\delta L_{int}=\int_{V}(\delta\boldsymbol{\epsilon}_{p}^{T}\boldsymbol{\sigma}_{p}+\delta\boldsymbol{\epsilon}_{n}^{T}\boldsymbol{\sigma}_{n})dV=\delta L_{ext} \qquad (38)
$$

where L_{int} stands for the strain energy, and L_{ext} is the work of the external loadings. δ stands for the virtual variation. The virtual variation of the strain energy is rewritten

using Equations (5), (8) and (37), in a compact format which becomes:

$$\delta L_{int} = \delta \mathbf{q}_{\tau i}^T \mathbf{K}^{ij\tau s} \mathbf{q}_{sj} \tag{39}$$

where $\mathbf{K}^{ij\tau s}$ is the stiffness matrix in the form of the fundamental nucleus. Its components are:

$$\begin{aligned}
K_{xx}^{ij\tau s} = {} & \tilde{C}_{22} \int_\Omega F_{\tau,x} F_{s,x} d\Omega \int_l N_i N_j dy + \tilde{C}_{66} \int_\Omega F_{\tau,z} F_{s,z} d\Omega \int_l N_i N_j dy + \\
& \tilde{C}_{44} \int_\Omega F_\tau F_s d\Omega \int_l N_{i,y} N_{j,y} dy \\
K_{xy}^{ij\tau s} = {} & \tilde{C}_{23} \int_\Omega F_{\tau,x} F_s d\Omega \int_l N_i N_{j,y} dy + \tilde{C}_{44} \int_\Omega F_\tau F_{s,x} d\Omega \int_l N_{i,y} N_j dy \\
K_{xz}^{ij\tau s} = {} & \tilde{C}_{12} \int_\Omega F_{\tau,x} F_{s,z} d\Omega \int_l N_i N_j dy + \tilde{C}_{66} \int_\Omega F_{\tau,z} F_{s,x} d\Omega \int_l N_i N_j dy \\
K_{yx}^{ij\tau s} = {} & \tilde{C}_{44} \int_\Omega F_{\tau,x} F_s d\Omega \int_l N_i N_{j,y} dy + \tilde{C}_{23} \int_\Omega F_\tau F_{s,x} d\Omega \int_l N_{i,y} N_j dy \\
K_{yy}^{ij\tau s} = {} & \tilde{C}_{55} \int_\Omega F_{\tau,z} F_{s,z} d\Omega \int_l N_i N_j dy + \tilde{C}_{44} \int_\Omega F_{\tau,x} F_{s,x} d\Omega \int_l N_i N_j dy + \\
& \tilde{C}_{33} \int_\Omega F_\tau F_s d\Omega \int_l N_{i,y} N_{j,y} dy \\
K_{yz}^{ij\tau s} = {} & \tilde{C}_{55} \int_\Omega F_{\tau,z} F_s d\Omega \int_l N_i N_{j,y} dy + \tilde{C}_{13} \int_\Omega F_\tau F_{s,z} d\Omega \int_l N_{i,y} N_j dy \\
K_{zx}^{ij\tau s} = {} & \tilde{C}_{12} \int_\Omega F_{\tau,z} F_{s,x} d\Omega \int_l N_i N_j dy + \tilde{C}_{66} \int_\Omega F_{\tau,x} F_{s,z} d\Omega \int_l N_i N_j dy \\
K_{zy}^{ij\tau s} = {} & \tilde{C}_{13} \int_\Omega F_{\tau,z} F_s d\Omega \int_l N_i N_{j,y} dy + \tilde{C}_{55} \int_\Omega F_\tau F_{s,z} d\Omega \int_l N_{i,y} N_j dy \\
K_{zz}^{ij\tau s} = {} & \tilde{C}_{11} \int_\Omega F_{\tau,z} F_{s,z} d\Omega \int_l N_i N_j dy + \tilde{C}_{66} \int_\Omega F_{\tau,x} F_{s,x} d\Omega \int_l N_i N_j dy + \\
& \tilde{C}_{55} \int_\Omega F_\tau F_s d\Omega \int_l N_{i,y} N_{j,y} dy
\end{aligned} \tag{40}$$

It should be noted that no assumptions on the approximation order have been done. It is therefore possible to obtain refined beam models without changing the formal expression of the nucleus components. This is the key-point of CUF which permits, with only nine FORTRAN statements, us to implement any-order beam theories. The shear locking is corrected through the selective integration (see [52]).

Virtual Variation of Inertial and External Loadings

The virtual variation of the work of the inertial loadings is:

$$\delta L_{ine} = \int_V \rho \ddot{\boldsymbol{u}} \delta \boldsymbol{u}^T dV \tag{41}$$

where ρ stands for the density of the material, and $\ddot{\boldsymbol{u}}$ is the acceleration vector. Equation 41 is rewritten using Equations 5, and 37:

$$\delta L_{ine} = \int_l \delta \mathbf{q}_{\tau i}^T N_i \left[\int_\Omega \rho (F_\tau \mathbf{I})(F_s \mathbf{I}) d\Omega \right] N_j \ddot{\mathbf{q}}_{sj} dy \tag{42}$$

where $\ddot{\boldsymbol{q}}$ is the nodal acceleration vector. The last equation can be rewritten in the following compact manner:

$$\delta L_{ine} = \delta \mathbf{q}_{\tau i}^T \mathbf{M}^{ij\tau s} \ddot{\mathbf{q}}_{sj} \tag{43}$$

where $\mathbf{M}^{ij\tau s}$ is the mass matrix in the form of the fundamental nucleus. Its components are:

$$\begin{gathered} M_{xx}^{ij\tau s} = M_{yy}^{ij\tau s} = M_{zz}^{ij\tau s} = \rho \int_\Omega F_\tau F_s d\Omega \int_l N_i N_j dy \\ M_{xy}^{ij\tau s} = M_{xz}^{ij\tau s} = M_{yx}^{ij\tau s} = M_{yz}^{ij\tau s} = M_{zx}^{ij\tau s} = M_{zy}^{ij\tau s} = 0 \end{gathered} \tag{44}$$

The undamped dynamic problem can be written as follows:

$$\boldsymbol{M}\ddot{\boldsymbol{a}} + \boldsymbol{K}\boldsymbol{a} = \boldsymbol{p} \tag{45}$$

where $\boldsymbol{a}$ is the vector of the nodal unknowns and $\boldsymbol{p}$ is the loadings vector. Introducing harmonic solutions, it is possible to compute the natural frequencies, ω_i, for the homogenous case, by solving an eigenvalues problem:

$$(-\omega_i^2 \mathbf{M} + \mathbf{K})\boldsymbol{a}_i = 0 \tag{46}$$

where $\boldsymbol{a}_i$ is the $i\text{-}th$ eigenvector.

The loading vector variationally coherent to the model is derived for the case of a generic concentrated load $\mathbf{P}$:

$$\mathbf{P} = \left\{ \begin{array}{ccc} P_{u_x} & P_{u_y} & P_{u_z} \end{array} \right\}^T \tag{47}$$

Any other loading condition can be similarly treated. The virtual work due to $\mathbf{P}$ is:

$$\delta L_{ext} = \mathbf{P} \delta \mathbf{u}^T \tag{48}$$

The virtual variation of $\mathbf{u}$ in the framework of CUF is:

$$\delta L_{ext} = F_\tau \mathbf{P} \delta \mathbf{u}_\tau^T \tag{49}$$

By introducing the nodal displacements and the shape functions, the previous equation becomes:

$$\delta L_{ext} = F_\tau N_i \mathbf{P} \delta \mathbf{q}_{\tau i}^T \tag{50}$$

This last equation permits the identification of the components of the nucleus which have to be loaded, that is, it permits the proper assembling of the loading vector by detecting the displacement variables that have to be loaded. In the case of first order expansion and **P** acting on a node along x direction only, the virtual external work is:

$$\delta L_{ext} = P_{u_x} \delta u_{x1} + x_p P_{u_x} \delta u_{x2} + z_p P_{u_x} \delta u_{x3} \tag{51}$$

where $[x_p,\ z_p]$ are the coordinates on the cross-section of the loading application point.

4 Results and Discussion

Several structural models are herein considered. Preliminary results concern the static and free vibration analysis of compact cross-section beams. More complex geometries are addressed afterwards. Particular attention is given to thin walled structures, such as hollow cylinders and wings, and bridge-like cross-sections. Isotropic and FGM materials are used. Various loading and boundary conditions are considered (*e.g.* bending, torsion, cantilevered, *etc.*). Comparisons of the results with analytical models and commercial finite element (FE) codes are provided.

4.1 Compact Square Cross-Section

A square cross-section beam made of isotropic material is considered. The geometry of the model is shown in Figure 4. b and h are assumed as high as 0.2 [m]. Two length-to-thickness ratios, L/h, are used: 100 and 10. Slender and moderately thick beams are therefore considered. The Young modulus, E, is equal to 75 [GPa]. The Poisson ratio, ν, is equal to 0.33. First the static analysis is addressed. The beam is cantilevered. A force, F_z, is applied at the free cross-section center point. F_z is assumed as high as -50 [N]. Table 2 shows the influence of the number of elements and

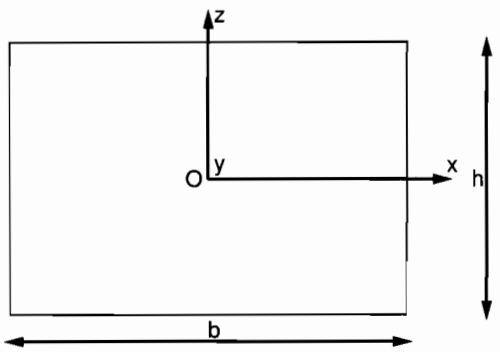

Figure 4: Rectangular cross-section

No. Elem.	EBBM	TBM	$N=1$	$N=2$	$N=3$	$N=4$
$L/h=100$, $u_z \times 10^2$ [m], $u_{z_b} \times 10^2 = -1.333$ [m]						
1	-1.334	-1.334	-1.334	-1.239	-1.239	-1.239
3	-1.334	-1.334	-1.334	-1.302	-1.302	-1.302
5	-1.334	-1.334	-1.334	-1.315	-1.315	-1.315
10	-1.334	-1.334	-1.334	-1.325	-1.325	-1.325
40	-1.334	-1.334	-1.334	-1.332	-1.332	-1.332
$L/h=10$, $u_z \times 10^5$ [m], $u_{y_b} \times 10^5 = -1.333$ [m]						
1	-1.334	-1.343	-1.343	-1.248	-1.250	-1.250
3	-1.334	-1.343	-1.343	-1.309	-1.311	-1.311
5	-1.334	-1.343	-1.343	-1.320	-1.322	-1.323
10	-1.334	-1.343	-1.343	-1.327	-1.329	-1.330
40	-1.334	-1.343	-1.343	-1.330	-1.332	-1.333

Table 2: Vertical displacement of the loaded point for different meshes and beam models [38]

of the beam theory on the vertical displacement of the loaded point. The benchmark value, u_{z_b}, has been obtained by using the Euler-Bernoulli theory. The torsion analysis is conducted by applying a torque as high as 50 [kN m] at the free tip. A 40 four-node element mesh is used. Table 3 shows the rotation values of the free section obtained for different beam models. The benchmark has been obtained as in [53].

	$L/h=100$	$L/h=10$
Benchmark	9.033	0.903
$N=1$	7.635	0.768
$N=2$	7.616	0.747
$N=3$	7.609	0.720
$N=4$	9.000	0.862

Table 3: Rotation of the free section, [deg], [38]

The free vibration analysis considers a simply-supported beam with the same material and geometric features as the static case. A 10 four-node mesh is adopted. Tables 4 and 5 report the first two bending frequencies for the slender and the thick beam, respectively. Increasing order beam models are considered. The reference solutions f_{1_b} and f_{2_b} have been obtained via the Euler-Bernoulli theory.

The following considerations can be made at the end of the structural analysis of the compact cross-section beam.

1. A general excellent agreement has been found between the results from the present formulation and the analytical benchmarks in terms of displacements and natural frequencies.

EBBM	TBM	$N=1$	$N=2$	$N=3$
		f_{1_b} = 1.195 [Hz]		
1.195	1.194	1.194	1.194	1.194
		f_{2_b} = 4.780 [Hz]		
4.778	4.775	4.775	4.775	4.775

Table 4: First two bending natural frequencies in the case of $L/h = 100$ [39]

EBBM	TBM	$N=1$	$N=2$	$N=3$	$N=4$
		f_{1_b} = 119.495 [Hz]			
118.968	117.701	117.701	117.728	117.526	117.525
		f_{2_b} = 477.978 [Hz]			
470.143	451.838	451.838	452.193	449.438	449.419

Table 5: First two bending natural frequencies in the case of $L/h = 10$ [39]

2. The use of a more refined mesh as well as higher-order models reduces the stiffness of the FE model.
3. The beneficial effect of the higher-order theories increases as the slenderness ratio decreases and the mode number increases.

4.2 Wing Models

Different wing models are analyzed. The static analysis is conducted on a three-cell cantilevered wing modeled via a fourth-order model. Figure 5 shows the geometry of the cross-section. A NACA 2415 profile has been used to define the contour of the wing. The chord, b, is equal to 1 [m]. L/b is assumed as high as 5. The torsion analysis

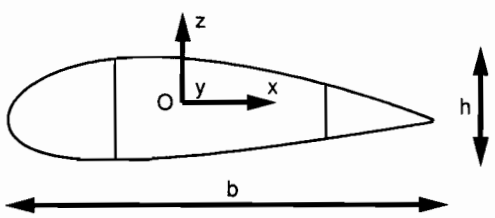

Figure 5: Wing cross-section

has been conducted by applying two opposite vertical forces, $\pm F_z$ at the leading and trailing edges of the free cross-section. The magnitude of the forces is equal to 5 [kN]. Figure 6 shows the deformed loaded cross-section. Unconventional wing geometries are considered as well. Figure 7 shows the geometric characteristics of the considered

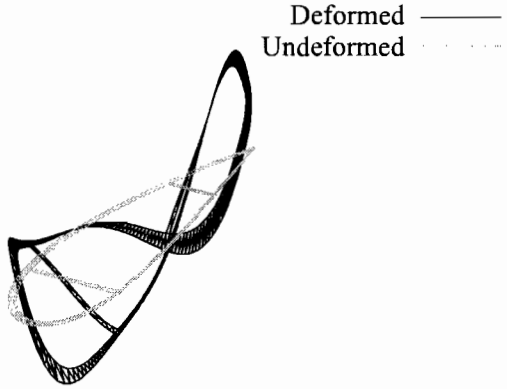

Figure 6: Deformed wing cross-section under a torsional load [38]

model. The cross-section is rectangular with b equal to 1 [m] and h equal to 0.1 [m] (Figure 4 shows the geometric characteristics of the cross-section). The length-to-thickness ratios, L_1/h and L_2/h, are equal to 100 and 30, respectively, with L_3 as high as L_1. The free vibration analysis is conducted and the results are compared with

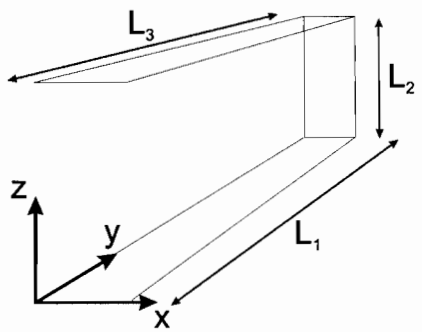

Figure 7: Geometry of the joined wing

those retrieved via a shell model in MSC Nastran. Forty-five four-node beam elements are used and a fourth-order theory is exploited. Figures 8 and 9 show a natural mode compared with the one by the shell solution.

The assessments on the wing models highlight the following statements.

1. The proposed beam formulation is able to deal with arbitrary cross-section geometries as well as unconventional configurations.
2. Refined models are able to detect non-classical effects such as the warping of a thin-walled structure.
3. Higher-order beam theories furnish results which are comparable with those given by more cumbersome shell models.

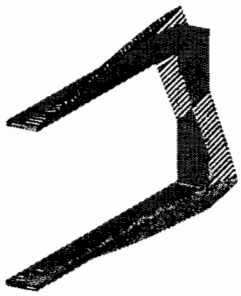

Figure 8: Natural mode of a joined wing. Beam model solution. $f = 47.512$ [Hz] [42]

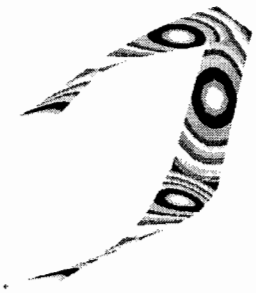

Figure 9: Natural mode of a joined wing. Shell model solution. $f = 47.118$ [Hz] [42]

4.3 Thin-Walled Structures

Different thin-walled structures are considered. Analytical and FE solutions are considered.

C-Shaped Cross-Section and Bending-Torsional Loading

Beams with a C-shaped cross-section are subjected to a uniform loading acting as shown in Figure 10. Closed-form solutions are considered. Loading and the points in which displacements and stresses presented in tabular form are evaluated are also presented there. Table 6 presents the out-of-plane displacement components for $L/a = 100$ and ten. Results are non-dimensionalised as follows:

	$L/a = 100$ $10^{-1} \times \overline{u}_y$	$L/a = 10$ $10^{-1} \times \overline{u}_y$
FEM 3D	-9.945	-3.528
N=15	-9.829	-3.502
N=8	-9.277	-3.293
N=5	-8.304	-1.830
N=3	-8.138	-0.878
N=1	-8.131	-0.820
TBM	-8.131	-0.813
EBBM	-8.131	-0.813

Table 6: Out-of-plane displacements for C-shaped beam, $L/a = 100$ and 10 [54]

$$(\overline{u}_x, \overline{u}_y, \overline{u}_z) = \frac{aE}{l^2 p_{xx}^{+1}} (u_x, u_y, u_z) \tag{52}$$

The deformed mid-span cross-section for $L/a = 10$ is shown in Figure 11. Colour

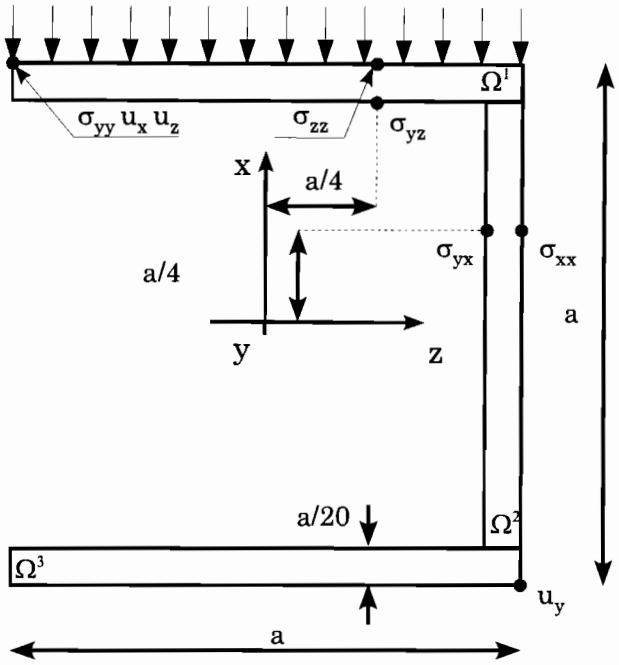

Figure 10: C-shaped cross-section geometry, loading and results verification points

maps of stress components are presented in Figures 12 and 13. For the sake of brevity, only deep beams are considered. The following considerations hold.

1. An accurate prediction of the out-of-plane displacement u_y calls for an eighth-order model at least.
2. The 15$^{\text{th}}$-order model describes accurately the in-plane warping. It differs from the FE solution only near the free end of the upper branch.
3. A 15$^{\text{th}}$-order model has been considered. Apart for stress concentration in correspondence of the internal corner points, results are very similar. High gradients of σ_{yx} are correctly modeled.

Thin-Walled Cylinder

First a thin-walled cylinder is considered. Both ends are clamped. The cross-section geometrical features are shown in Figure 14. The thickness of the structure is equal to 0.02 [m], the diameter, d, is equal to 2 [m], and the length-to-diameter ratio, L/d, is as high as 10. The static analysis is assessed by applying a point load, F_z, at [0, $L/2$, 1]. F_z is equal to -5.0 [MN]. Table 7 shows the vertical displacement of the loaded point obtained through different beam theories. A shell model is used to compare the results. The second column reports the total number of degrees of freedom of each model.

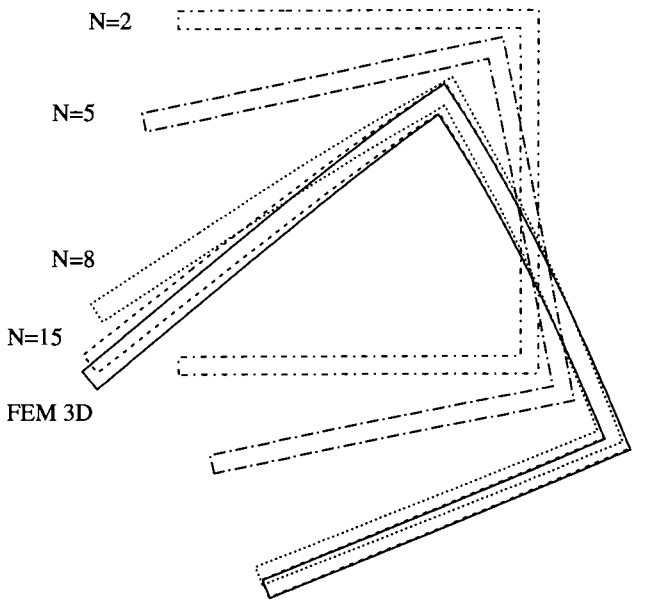

Figure 11: In-plane warping of C-shaped beam cross-section at mid-span, $L/a = 10$ [54]

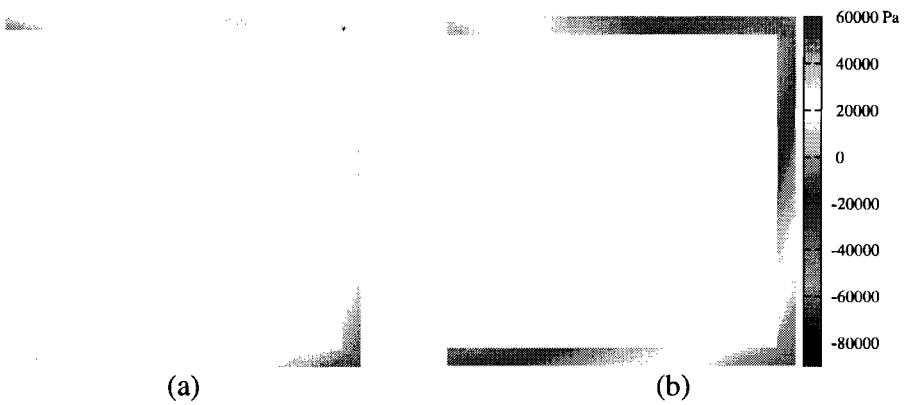

Figure 12: Dimensionalised stress σ_{yy} (Pa) above the cross section for C-shaped beam at mid-span via (a) FE solution and (b) 15^{th}-order model, $L/a = 10$ [54]

Figure 15 shows the deformed configurations of the cylinder for different beam theories. A two-dimensional sketch of the deformed loading point cross-section is shown in Figure 16 where results from beam theories and a shell model are compared. Table 8 reports the first two natural bending frequencies of the considered structure. Increasing order beam theories as well as shell and solid models are used. Superscripts indicate the position of each frequency within the eigenvalue vector. Figures 17 and 18 present two natural modes which show lobes along the circumferential direction.

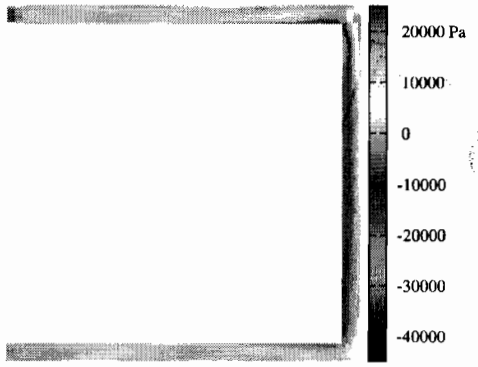

(a) (b)

Figure 13: Dimensionalised stress σ_{yx} (Pa) above the cross section for C-shaped beam at $y = 0$ via (a) FE solution and (b) 15^{th}-order model, $L/a = 10$ [54]

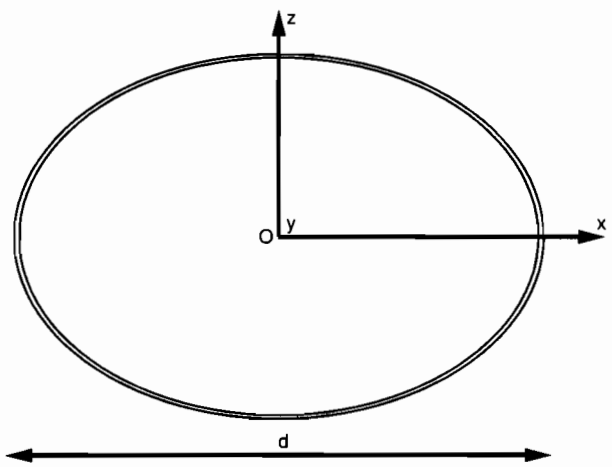

Figure 14: Geometry of the annular cross-section

The first three-lobe frequency is reported in Table 9 for different beam, shell, and solid models.

The analysis of the thin-walled cylinder has highlighted several important features of the present beam formulation.

1. Classical and lower-order beam models are not able to furnish reliable results whenever important cross-section deformations are present.
2. Refined models can detect results that are usually obtainable just by means of shell or solid models, that is, shell-like results can be obtained by means of beam elements.
3. The bending frequencies are well computed by the third-order model. The

Theory	DOF's	u_z [m]
EBBM	155	−0.046
TBM	155	−0.053
N = 1	279	−0.053
N = 2	558	−0.052
N = 3	930	−0.114
N = 4	1395	−0.229
N = 5	1953	−0.335
N = 6	2604	−0.386
N = 7	3348	−0.486
N = 8	4185	−0.535
N = 9	5115	−0.564
N = 10	6138	−0.584
N = 11	7254	−0.597
Shell	49500	−0.670

Table 7: Vertical displacement of the loading point for different beam theories and comparison with a shell model [40]

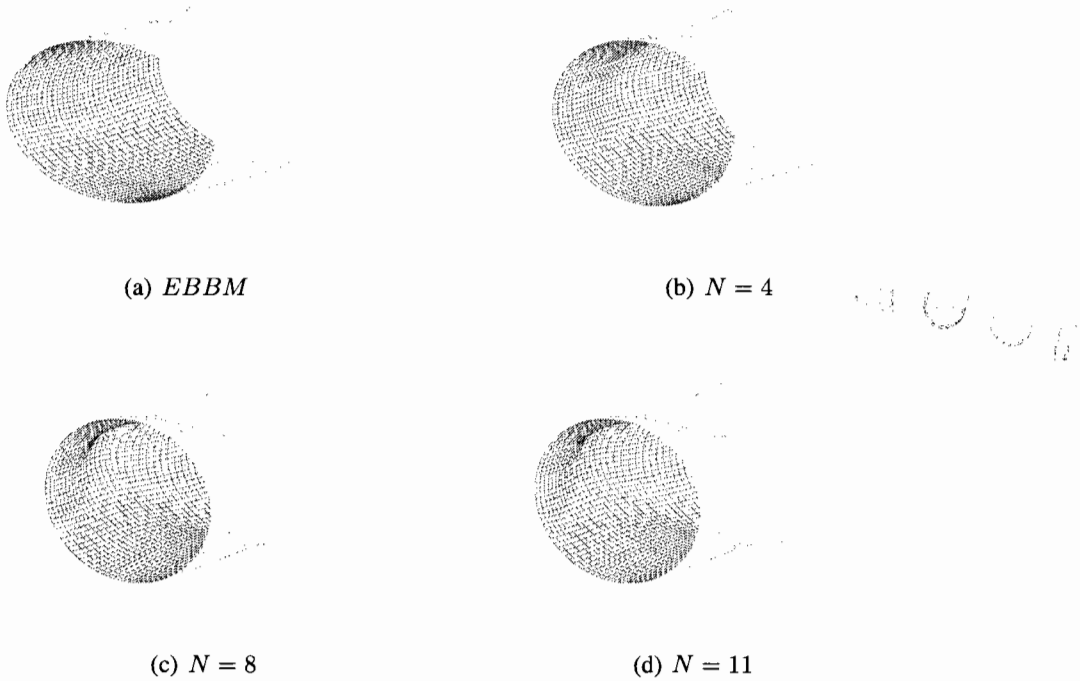

(a) $EBBM$ (b) $N = 4$

(c) $N = 8$ (d) $N = 11$

Figure 15: Deformed configurations of the thin-walled cylinder for various theories [40]

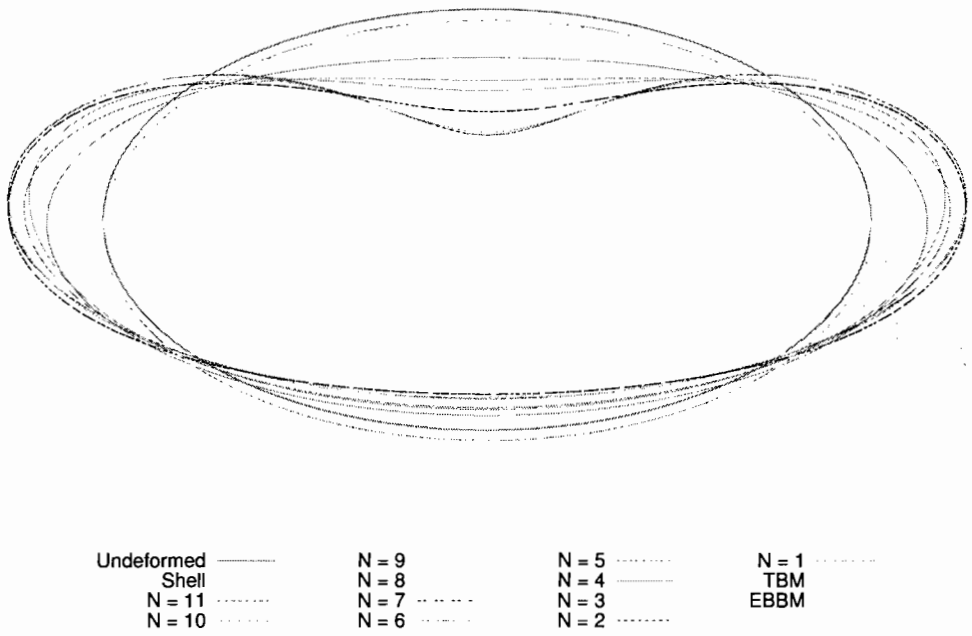

Figure 16: Deformed configurations of the loading point cross-section for different beam theories and comparison with a shell model [40]

Theory	DOF's	f_1 [Hz]	f_2 [Hz]
EBBM	155	$32.598^{1,2*}$	$88.072^{3,4}$
TBM	155	$30.304^{1,2}$	$76.447^{3,4}$
N = 1	279	$30.304^{1,2}$	$76.447^{3,4}$
N = 2	558	$30.730^{1,2}$	$77.338^{3,4}$
N = 3	930	$28.754^{1,2}$	$69.448^{5,6}$
N = 4	1395	$28.747^{3,4}$	$69.402^{9,10}$
N = 5	1953	$28.745^{3,4}$	$69.397^{13,14}$
N = 6	2604	$28.745^{3,4}$	$69.397^{17,18}$
Shell	49500	$28.489^{3,4}$	$68.940^{17,18}$
Solid	174000	$28.369^{3,4}$	$68.687^{17,18}$

$(*)$: positions of the frequencies in the eigenvalue vector

Table 8: First two bending frequencies of the thin-walled cylinder for different beam, shell, and solid models [40]

(a) Two lobes (b) Three lobes

Figure 17: Circumferential natural modes, three-dimensional view, [40]

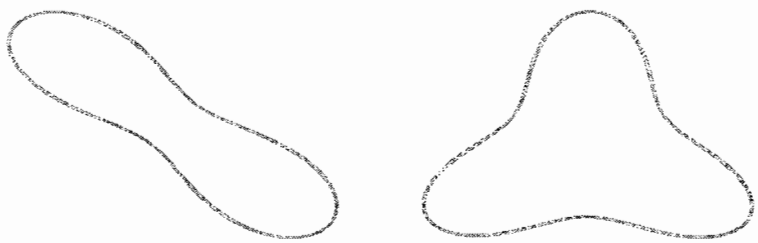

(a) Two lobes (b) Three lobes

Figure 18: Circumferential natural modes, two-dimensional view, [40]

Theory	DOFs	f [Hz]
EBBM	155	–
TBM	155	–
N = 1	279	–
N = 2	558	–
N = 3	930	–
N = 4	1395	75.690
N = 5	1953	65.186
N = 6	2604	52.386
N = 7	3348	50.372
N = 8	4185	40.102
Shell	49500	40.427
Solid	174000	46.444

Table 9: First three-lobe frequency [40]

proper detection of more sophisticated modal shapes or the presence of point loads require the use of even higher-order models.

4. The computational effort of a higher-order beam model is significantly lower than the ones requested by shell or solid models.

4.4 Bridge-Like Cross-Section and Discussion on the Shear Correction Factor

A bridge-like structure is considered herein. Figure 19 shows the geometric characteristics of the cross-section. The dimensions of the structure are reported in Table 10. Steel is used as the material, with E as high as 210 [GPa], and ν equal to 0.3. A uniform distributed load, P_S, is applied at the top surface of the beam. P_S is equal to 10 [kPa]. The beam is considered clamped-clamped. An MSC Nastran solid model is used for comparison purposes. Figures 20 show the vectorial distribution of the

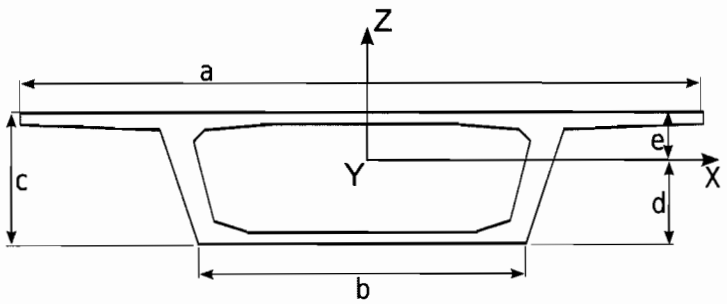

Figure 19: Geometry of the bridge-like cross-section [46]

	[m]
a	15.200
b	3.450
c	1.450
d	2.155
e	1.295
L	100

Table 10: Bridge-like cross-section dimensions [46]

transverse shear stress for different beam models. A comparison in terms of stress fields between the present beam and solid elements is given in Figure 21.

Shear correction factors are computed as in [47], K^C, and [48,49], K^G. The Poisson's ratio is set equal to 0.2. Table 11 shows the values obtained with a comparison with those from open literature. The static analysis of the bridge-like beam permit us to underline what follows.

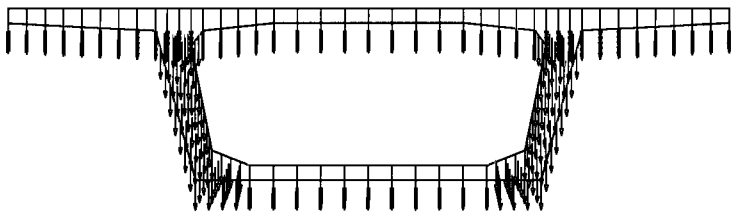

(a) $\sigma_{xy} + \sigma_{zy}$, TBM

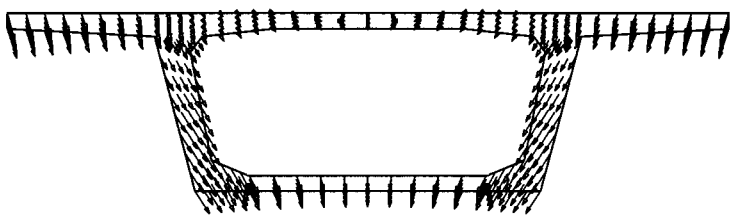

(b) $\sigma_{xy} + \sigma_{zy}$, $N = 2$

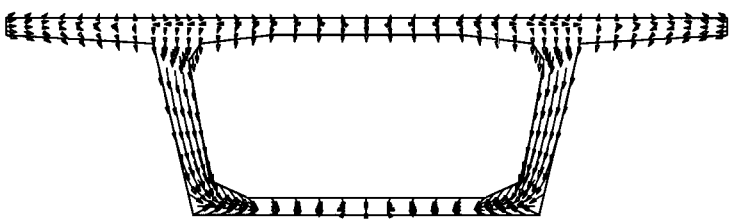

(c) $\sigma_{xy} + \sigma_{zy}$, $N = 4$

Figure 20: Vectorial shear stress distribution at $y = L/4$ for different beam theories [43]

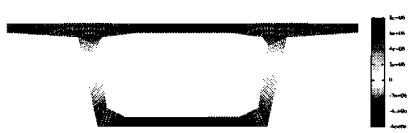

(a) σ_{yy}, $N = 4$

(b) σ_{yy}, Solid

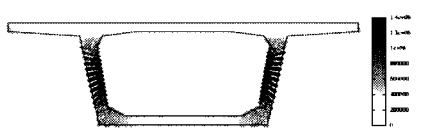

(c) $\sigma_{xy} + \sigma_{zy}$, $N = 4$

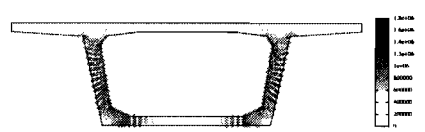

(d) $\sigma_{xy} + \sigma_{zy}$, Solid

Figure 21: Comparison of stress fields, [Pa], between the fourth-order beam and solid elements [43]. $y = L/2$

	K_z	K_x
K^C		
$N=1$	1.000	1.000
$N=2$	0.681	0.961
$N=3$	0.331	0.707
$N=4$	0.320	0.689
K^G		
$N=1$	1.000	1.000
$N=2$	0.672	0.963
$N=3$	0.330	0.699
$N=4$	0.317	0.681
Sol. [46]	0.231	0.599

Table 11: Shear correction factors for the bridge-like cross-section [43]

1. The enhanced capabilities of higher-order beam models are necessary to investigate the stress field distribution of an arbitrary cross-section structure. The transverse shear stress components are those which are more sensitive to the use of higher-order models.
2. Refined one-dimensional beam models are able to offer good agreement with the results from three-dimensional solid element analysis with a significant reduction of computational and implementation costs.
3. The use as well as the definition of shear correction factors appears very much questionable as has been pointed out by many authors: its definition is a problem dependent parameter. The adoption of refined theories, in fact, offers a more flexible approach that is independent of the features of the addressed structural problem.

4.5 Beams made of FGM materials

Beams made of FGM materials are considered herein. Two cases are accounted for: a beam undergoing a bending load and a beam undergoing a torsion-bending load.

Beam under Bending Loading

A square cross-section is considered, see Figure 22. Dimension a along x and z axes equals 0.1 m. Deep beams ($L/a = 5$) are investigated. A unit maximal amplitude (1 MPa) for the surface loading is assumed. The material exhibits a gradation along both x and z directions: $E_0 = 1000$ MPa, α_i such that $E(a,0)/E_0 = E(0,a)/E_0 = 3$ and $\beta_i = 0$ with $i = 1$ and 2. Poisson's ratio equals 0.3. The proposed models are compared with a three-dimensional FE solution (denoted FEM 3D) developed using the MSC.Nastran commercial code. The eight-node brick element "HEXA8" is used. Element sides measure $2 \cdot 10^{-3}$ m. Each element is considered as homogeneous by

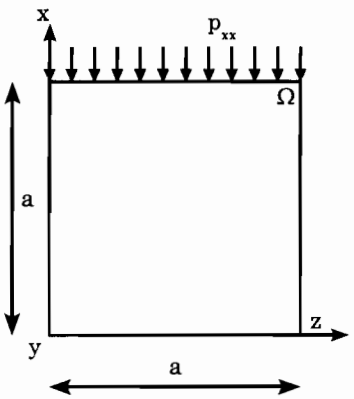

Figure 22: Square cross-section geometry and loading, beam made of FGM materials under bending loading

referring to the material properties at its center point.

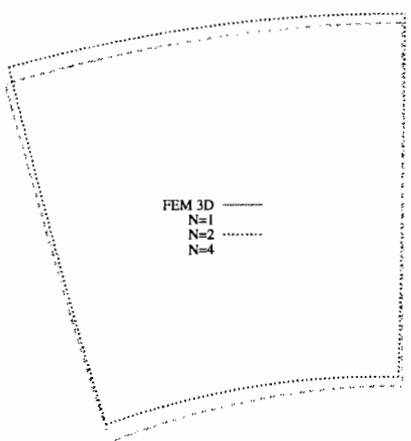

Figure 23: In-plane warping at $y/L = 0.5$ [55]

Figure 23 presents the cross-section deformation at $y/L = 0.5$. The shape of the deformation is due to the Young modulus variation law. Figs. 24 and 25 show the bending stress component σ_{yy}. Results are computed at beam mid-span. The maps of the shear stress component σ_{yx} are presented in Figs. 26 and 27. A fifth-order model has been used. The following considerations can be drawn.

1. The fourth-order model matches the reference FE solution in terms of displacements.
2. A first-order model yields an accurate description of the bending stress component σ_{yy}. A fifth-order model is needed to detect the shear stress distribution.

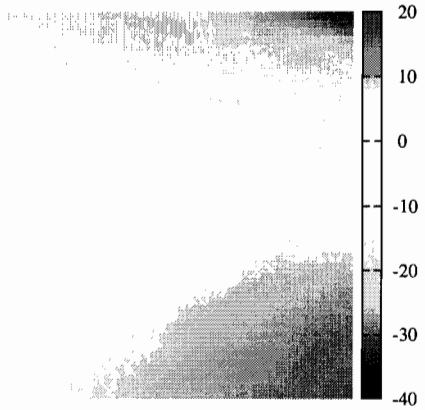

Figure 24: σ_{yy} (MPa) at mid-span via FEM 3D [55]

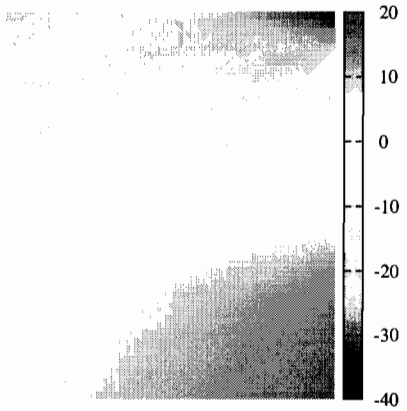

Figure 25: σ_{yy} (MPa) at mid-span via first-order model [55]

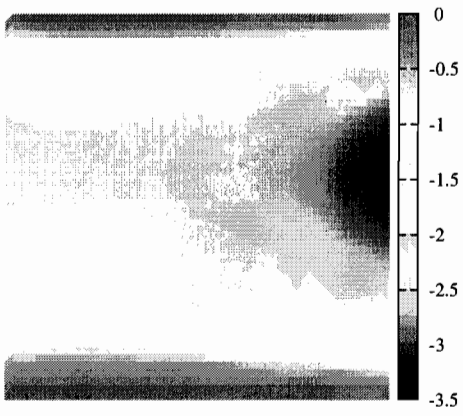

Figure 26: σ_{yx} (MPa) at $y/L = 0$ via FEM 3D [55].

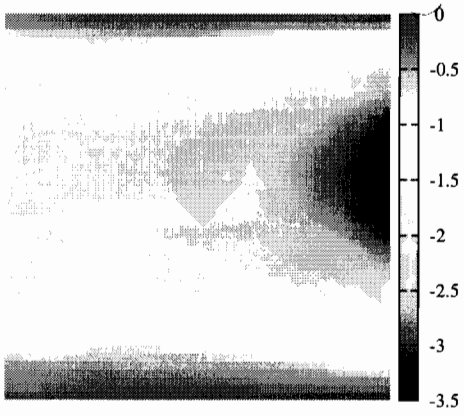

Figure 27: σ_{yx} (MPa) at $y/L = 0$ via fifth-order model [55].

3. As far as the computational time is concerned, the proposed analytical models require less than a second, regardless of the approximation order. The FE solution based on the proposed models, not reported here, is obtained in a few seconds for a very fine mesh. For the reference FEM 3D solution, the computational time is about five minutes.

Beam under Bending-Torsion Loading

A beam with a square cross-section subjected to a line loading is investigated. Cross-section sides measure 100 [mm]. The span-to-height ratio is equal to 5. The loading configuration and reference system are shown in Figure 28. Maximal loading ampli-

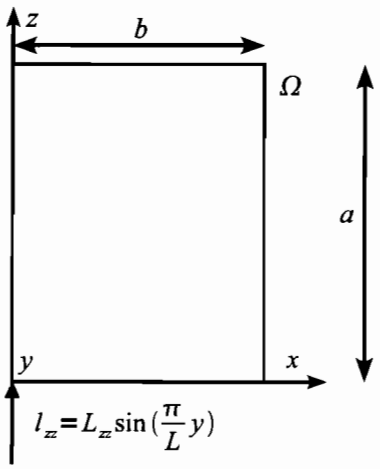

Figure 28: Beam subjected to bending-torsion

tude is L_{zz} and m equals the unity. The material exhibits a gradation along both x and z directions: $E_0 = 1000$ N/mm^2, α_i such that $E(b,0)/E_0 = E(0,a)/E_0 = 3$ and $\beta_i = 0$ with $i = 1$ and 2. Poisson's ratio equals 0.3. Stress components are normalized with respect to the ratio between the cross-section area and the loading resultant:

$$(\overline{\sigma}_{xx}, \overline{\sigma}_{xz}, \overline{\sigma}_{xy}, \overline{\sigma}_{yy}, \overline{\sigma}_{zz}) = \frac{\pi}{2}\frac{ab}{L\, L_{zz}}(\sigma_{xx}, \sigma_{xz}, \sigma_{xy}, \sigma_{yy}, \sigma_{zz}) \tag{53}$$

The normal stress component $\overline{\sigma}_{yy}$ is evaluated at $(b, L/2, 0)$. Shear stresses $\overline{\sigma}_{yz}$ and $\overline{\sigma}_{yx}$ are computed at $(0, 0, a/2)$ and $(b/2, 0, a)$, respectively. Components $\overline{\sigma}_{xx}$ and $\overline{\sigma}_{zz}$ are evaluated at $(4b/25, L/2, 0)$ and $(0, L/2, 3a/25)$, respectively. The proposed models are compared with a three-dimensional FE solution developed using the MSC.Nastran commercial code. The eight-node brick element "HEXA8" is used. Two element sizes are considered: $4 \times 2 \times 2$ mm (FEM 3D^b) and $4 \times 4 \times 4$ mm (FEM 3D^c). The three dimensions of each element are equal to 2 (FEM 3D^d), 4 (FEM 3D^c) mm. Each element is considered as homogeneous by referring to the material properties at its center point.

Figure 29 presents the deformation of the cross-section at mid-span for $L/a = 5$. Table 12 presents the dimensionless stresses for $L/a = 5$. For solution FEM 3D^c, shear stresses are computed as an average between two consecutive nodes since the stresses are calculated at the element's center and they are extrapolated out to the corner points only. The sudden change in slope in the neighborhood of the loading application area is due to the presence of a high displacement gradient. A higher

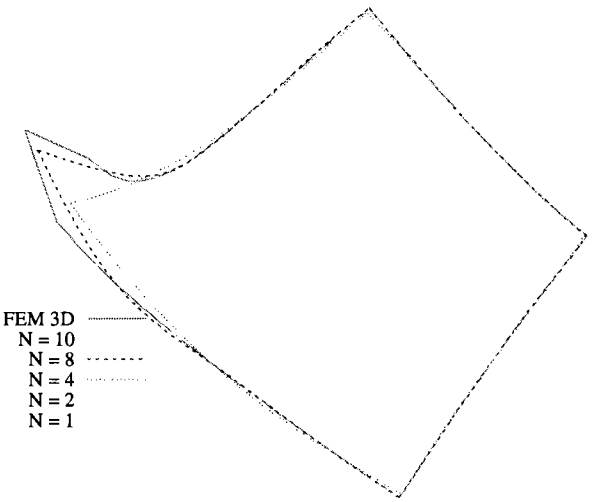

Figure 29: Cross-section deformation at $y = L/2$ for $L/a = 5$, beam under bending-torsion loading [56]

	$\overline{\sigma}_{yy}$	$\overline{\sigma}_{xx}$	$\overline{\sigma}_{zz}$	$\overline{\sigma}_{yz}$	$\overline{\sigma}_{yx}$
FEM 3D[d]	−5.5559	2.6328	−5.4280	1.4465	1.9920
FEM 3D[c]	−5.5550	2.6675	−5.5675	1.4586⋆	1.9658⋆
N = 8	−5.6420	2.5120	−5.6689	1.4173	2.0032
N = 7	−5.5082	2.0114	−4.8488	1.4440	2.0243
N = 6	−5.5341	1.5355	−3.9423	1.4544	2.0409
N = 5	−5.7766	1.0784	−2.9782	1.4762	2.0797
N = 4	−5.6257	0.6734	−2.0170	1.4589	2.0510
N = 3	−5.3970	0.3021	−1.1304	1.0628	1.3239
N = 2	−5.3173	0.0961	−0.4096	0.9401	1.2334
N = 1	−5.3332	0.0164	−0.0660	0.8510	1.1875
TB	−6.1078	–	–	0.2568	−0.0939

Elements' sides length: FEM 3D[d] 2 × 2 × 2 mm; FEM 3D[c] 4 × 4 × 4 mm.
(⋆) Average value of two consecutive nodes.

Table 12: Dimensionless stresses for $L/a = 5$, bending-torsion loading [56].

number of nodes is required in that area in order to obtain a variation that is smoother and closer to the actual behavior. The analysis of the beam undergoing a bending-torsion loading highlights the following statements.

1. A tenth-order model yields very good results compared with solution FEM 3D[c] in terms of displacements.
2. Good results are obtained for the normal and shear stress components, being the difference versus the three-dimensional solutions about 2% for $N = 8$, at worse.

3. In the case of the transverse normal stress components, the difference is about 5%. This is due to the fact that such components are computed in the neighborhood of the loading application area and the stress field is highly three-dimensional. The two reference FE solutions differ there by about 2.5%. In this case a layer-wise approach is required. In such models, the displacement field is locally approximated. This will be a matter for further development of the proposed approach to the one-dimensional modeling.
4. As far as the computational costs are concerned, the proposed analytical models require less than a second, regardless the approximation order. The FE solution based on the proposed models, not reported here for the sake of brevity, is obtained in few seconds for a very fine mesh. For the reference three-dimensional FE solutions, FEM $3D^d$ requires about two hours, while for FEM $3D^c$ results have been obtained after two minutes.

4.6 Effectiveness Analysis of Higher-Order Terms

The present unified beam formulation permits us to comprehend the role of each term of a refined theory on a given structural problem. The investigation approach together with several results have been presented in detail in [41]. Each term is deactivated in turn and the effect of its absence is evaluated in terms of displacement and stress components. If the absence of a term does not corrupt the solution with respect to a reference value, the term itself will be considered as noneffective in computing the solution for the considered structural problem. The bending analysis is considered herein. A compact rectangular cross-section is considered first. The displacement field which is able to detect a full fourth-order solution in terms of displacement components is the following:

$$\begin{aligned} u_x &= xz\ u_{x_5} + x^3 z\ u_{x_{12}} + xz^3\ u_{x_{14}} \\ u_y &= z\ u_{y_3} + x^2 z\ u_{y_8} + z^3\ u_{y_{10}} \\ u_z &= u_{z_1} + z^2\ u_{z_6} + x^4\ u_{z_{11}} + x^2 z^2\ u_{z_{13}} + z^4\ u_{z_{15}} \end{aligned} \tag{54}$$

In other words, only 11 terms are effective in determining the displacement field of a compact beam undergoing a bending loading. The beam theory described by Equation 54 is graphically represented in Table 13 where the black symbols indicate the active terms of the fourth-order model. M_{eff} states the number of active terms.

A thin-walled structure is considered as a second assessment. The related set of active terms is given by:

$$\begin{aligned} u_x = \ & u_{x_1} + x\ u_{x_2} + x^2\ u_{x_4} + xz\ u_{x_5} + z^2\ u_{x_6} + x^3\ u_{x_7} + xz^2\ u_{x_9} + z^3\ u_{x_{10}} \\ & + x^4\ u_{x_{11}} + x^3 z\ u_{x_{12}} + + x^2 z^2\ u_{x_{13}} + xz^3\ u_{x_{14}} + z^4\ u_{x_{15}} \\ u_y = \ & u_{y_1} + z\ u_{y_3} + x^2\ u_{y_4} + xz\ u_{y_5} + z^2\ u_{y_6} + x^3\ u_{y_7} + x^2 z\ u_{y_8} + z^3\ u_{y_{10}} \\ & + x^4\ u_{y_{11}} + x^2 z^2\ u_{y_{13}} + + z^4\ u_{y_{15}} \\ u_z = \ & u_{z_1} + z\ u_{z_3} + x^2\ u_{z_4} + xz\ u_{z_5} + z^2\ u_{z_6} + x^2 z\ u_{z_8} + xz^2\ u_{z_9} + x^4\ u_{z_{11}} \\ & + x^3 z\ u_{z_{12}} + x^2 z^2\ u_{z_{13}} + + xz^3\ u_{z_{14}} + z^4\ u_{z_{15}} \end{aligned} \tag{55}$$

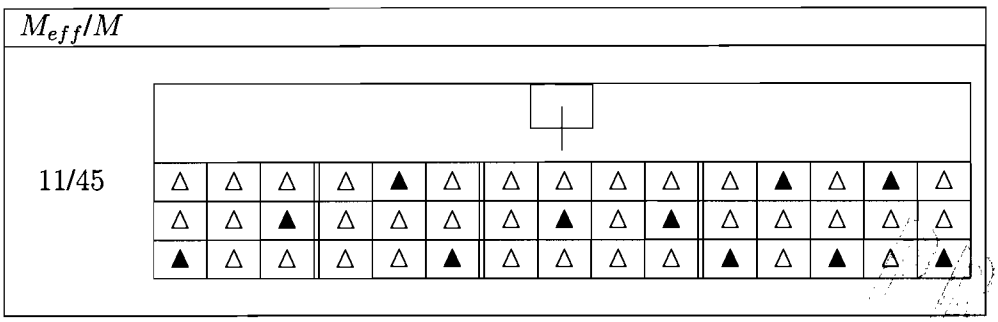

Table 13: Active displacement variables for a compact cross-section beam undergoing a bending load [41]

Table 14 shows the graphical version of the beam theory considered.

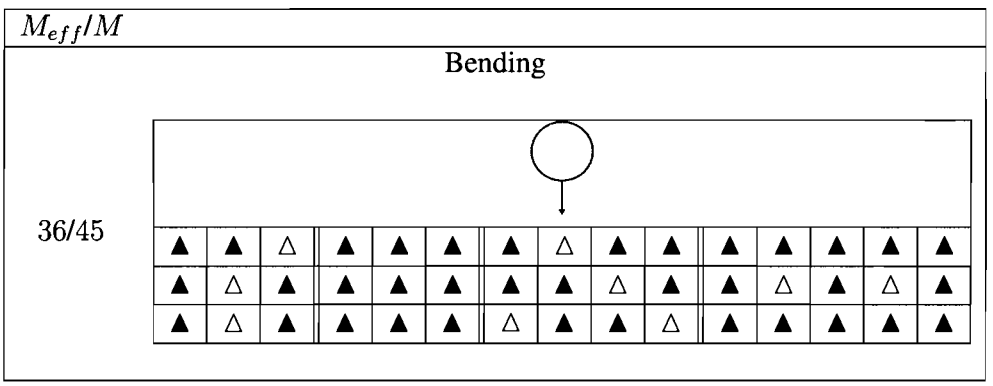

Table 14: Active displacement variables for different loading cases and cross-sections [41]

Similar analyses have been conducted on several structural cases (*e.g.* torsion and traction loads, slender and short beams, *etc.*). The results from the effectiveness analysis suggests what follows.

1. The set of active terms depends on the given structural problem, this dependence is extremely strong.
2. An important increase of terms is observed whenever thin-walled structures as well as torsional loading conditions are considered.
3. A set which is able to detect an output variable can be unable to predict another one, that is, if different outputs are requested different beam theories should be used.
4. All these aspects make the use of full refined theories more attractive in most of the cases.

5 Conclusion

This chapter has presented a unified formulation for higher-order beam theories. Refined models have been obtained by employing the Carrera unified formulation (CUF) which permits us to deal with any-order of beam theories without need of *ad hoc* implementations. In other words, the order of the theory is considered as an input of the analysis. Classical models (Euler-Bernoulli and Timoshenko) have been obtained as particular cases of the linear model. Closed form, Navier type solution and finite element formulations have been adopted. Arbitrary cross-section geometries have been considered. Static and free vibration analyses have been conducted. Isotropic and FGM materials have been used. The results obtained have been compared with those available from literature, with analytical approaches, and shell/solid finite element models.

The proposed unified approach has shown its strength in dealing with several different structural problems. There are several important features to be pointed out.

1. Higher order beam models are mandatory in the case of: short beams, thin-walled structures, FGM constitutive materials.
2. The use of refined beam models allows us to obtain detailed displacement and stress fields.
3. A wide set of non-classical effects can be detected (*e.g.* in- and out-of-plane warping, bending/torsion coupling, shear effects, *etc.*).
4. The results are in excellent agreement with those furnished by shell and solid elements.
5. The computational cost is particularly low with respect to the ones requested by shell and solid element models.

The adoption of refined theories offers a flexible approach that is independent of the features of the addressed structural problem. CUF makes this approach particularly attractive since its hierarchical capabilities, together with the possibility of addressing arbitrary geometries, permit us easily to obtain results which are usually furnished by more cumbersome two- or three-dimensional models. Future investigations could be directed towards considering aeroelastic applications and dynamic responses.

Acknowledgements

The first and third authors acknowledge the financial support from the Regione Piemonte project MICROCOST. The second author is supported by the Ministère de la Culture, de l'Enseignement Supérieuer et de la Recherche of Luxembourg via the project FNR CORE 2009 C09/MS/05 FUNCTIONALLY.

References

[1] R. Ballarini, "The Da Vinci-Euler-Bernoulli beam theory?", Mechanical Engineering Magazine, 2003. http://www.memagazine.org/

[2] L. Euler, "De curvis elasticis", Bousquet, Lausanne and Geneva, 1744.

[3] D. Bernoulli, "De vibrationibus et sono laminarum elasticarum", Commentarii Academiae Scientiarum Imperialis Petropolitanae, 1751.

[4] A.L. Cauchy, "Sur l'équilibre et le mouvement d'une plaque solide", Exercises de Matematique, 3, 328–355, 1828.

[5] S.D. Poisson, "Memoire sur l'équilibre et le mouvement des corps elastique", Mem. Acad. Sci., 1829.

[6] G. Kirchhoff, "Uber das gleichgewicht und die bewegung einer elastischen scheibe", J. Angew. Math., 40, 51–88, 1850.

[7] A. De Saint-Venant, "De la torsion des prismes, avec des considérations sur leur flexion, ainsi que sur l'équilibre des solides élastiques en général, et des formules pratiques pour le calcul de leur résistance à divers efforts s'exerçant simultanément", V. Dalmont, 1855.

[8] S.P. Timoshenko, "On the corrections for shear of the differential equation for transverse vibrations of prismatic bars", Philosophical Magazine, 41, 744–746, 1921.

[9] S.P. Timoshenko, "On the transverse vibrations of bars of uniform cross section", Philosophical Magazine, 43, 125–131, 1922.

[10] A.E.H. Love, "The Mathematical Theory of Elasticity", Fourth ed., Cambridge Univ Press, 1927.

[11] E. Reissner, "The effect of transverse shear deformation on the bending of elastic plates", ASME J. Appl. Mech., 12, 69–76, 1945.

[12] R.D. Mindlin, "Influence of rotatory inertia and shear in flexural motions of isotropic elastic plates", ASME J. Appl. Mech., 18, 1031–1036, 1950.

[13] B.F. Vlasov, "On the equations of bending of plates", Dokla Ak Nauk Azerbeijanskoi-SSR, 3, 955–979, 1957.

[14] W. Yu, V.V. Volovoi, D.H. Hodges, X. Hong, "Validation of the variational asymptotic beam sectional analysis (VABS)", AIAA Journal, 40, 2105–2113, 2002.

[15] E. Carrera, G. Giunta, "Refined beam theories based on Carrera's unified formulation", International Journal of Applied Mechanics, 2(1), 117–143, 2010.

[16] W.T. Koiter, "A consistent first approximation in the general theory of thin elastic shells", Proc. Kon. Ned. Ak. Wet., 612–619, 1961.

[17] H. Kraus, "Thin elastic shells", John Wiley, NY, 1967.

[18] P. Cicala, "Systematic approximation approach to linear shell theory", Levrotto e Bella, Torino, 1965.

[19] A.L. Gol'denweizer, "Derivation of an approximate theory of bending of a plate by the method of asymptotic integration of the equations of the theory of elasticity", Prikl. Mat. Mekh., 26, 1000–1025, 1962.

[20] E. Carrera, "Theories and finite elements for multilayered, anisotropic, compos-

ite plates and shells", Archives of Computational Methods in Engineering, 9(2), 87–140, 2002.

[21] E. Carrera, "Theories and finite elements for multilayered plates and shells: a unified compact formulation with numerical assessment and benchmarking", Archives of Computational Methods in Engineering, 10(3), 216–296, 2003.

[22] K. Kapania, S. Raciti, "Recent advances in analysis of laminated beams and plates, part I: Shear effects and buckling", AIAA Journal, 27(7), 923–935, 1989.

[23] K. Kapania, S. Raciti, "Recent advances in analysis of laminated beams and plates, part II: Vibrations and wave propagation", AIAA Journal, 27(7), 935–946, 1989.

[24] L. Librescu, O. Song, "On the static aeroelastic tailoring of composite aircraft swept wings modelled as thin-walled beam structures", Composites Engineering, 2, 497–512, 1992.

[25] S.J. Song, A.M. Waas, "Effects of shear deformation on buckling and free vibration of laminated composite beams", Composite Structures, 37(1), 33–43, 1997.

[26] J.R. Banerjee, F.W. Williams, "Coupled bending-torsional dynamic stiffness matrix for Timoshenko beam elements", Computers and Structures, 42(3), 301–310, 1992.

[27] V.V. Volovoi, D.H. Hodges, V.L. Berdichevsky, V.G. Sutyrin, "Asymptotic theory for static behavior of elastic anisotropic I-beams", International Journal of Solid Structures, 36, 1017–1043, 1999.

[28] V.V. Volovoi, D.H. Hodges, "Theory of anisotropic thin-walled beams", Journal of Applied Mechanics, 67, 453–459, 2000.

[29] B. Popescu, D.H. Hodges, "On asymptotically correct Timoshenko-like anisotropic beam theory", International Journal of Solids and Structures, 37, 535–558, 2000.

[30] W. Yu, D.H. Hodges, V.V. Volovoi, C.E.S. Cesnik, "On Timoshenko-like modeling of initially curved and twisted composite beams", International Journal of Solids and Structures, 39, 5101–5121, 2002.

[31] W. Yu, D.H. Hodges, "Elasticity solutions versus asymptotic sectional analysis of homogeneous, isotropic, prismatic beams", Journal of Applied Mechanics, 71, 15–23, 2004.

[32] W. Yu, D.H. Hodges, "Generalized Timoshenko theory of the variational asymptotic beam sectional analysis", Journal of the American Helicopter Society, 50(1), 46–55, 2005.

[33] E. Carrera, "A class of two-dimensional theories for anisotropic multilayered plates analysis", Atti della accademia delle scienze di torino. classe di scienze fisiche matematiche e naturali, 19–20, 1–39, 1995.

[34] E. Carrera, "Evaluation of layer-wise mixed theories for laminated plates analysis", AIAA Journal, 26, 830–839, 1998.

[35] E. Carrera, "Multilayered shell theories that account for a layer-wise mixed description. Part I: Governing equations", AIAA Journal, 37, 1107–1116, 1999.

[36] E. Carrera, "Multilayered shell theories that account for a layer-wise mixed de-

scription. Part II: Numerical evaluations", AIAA Journal, 37, 1117–1124, 1999.
[37] E. Carrera, M. Petrolo, "Guidelines and Recommendations to Construct Refinements of Classical Theories for Metallic and Composite Plates", AIAA Journal, In Press.
[38] E. Carrera, G. Giunta, P. Nali, M. Petrolo, "Refined beam elements with arbitrary cross-section geometries", Computers and Structures, 88(5–6), 283–293, 2010. doi:10.1016/j.compstruc.2009.11.002
[39] E. Carrera, M. Petrolo, P. Nali, "Unified formulation applied to free vibrations finite element analysis of beams with arbitrary section", Shock and Vibrations, 17, 1–18, 2010. doi:10.3233/SAV-2010-0528
[40] E. Carrera, M. Petrolo, "A beam formulation with shell capabilities", In "51st AIAA/ASME/ASCE/AHS/ASC Structures, Structural Dynamics, and Materials Conference", 2010.
[41] E. Carrera, M. Petrolo, "On the effectiveness of higher-order terms in refined beam theories", Journal of Applied Mechanics, In Press.
[42] E. Carrera, M. Petrolo, A. Varello, "Advanced Beam Formulations for Free Vibration Analysis of Conventional and Joined Wings", Submitted.
[43] E. Carrera, M. Petrolo, E. Zappino, "Advanced Elements for the Static Analysis of Beams with Compact and Bridge-Like Sections", Submitted.
[44] E. Carrera, G. Giunta, "Hierarchical closed form solutions for plates bent by localized transverse loadings", Journal of Zhejiang University SCIENCE A, 8(7), 1026–1037, 2007.
[45] E. Carrera, G. Giunta, "Hierarchical models for failure analysis of plates bent by distributed and localized transverse loadings", Journal of Zhejiang University SCIENCE A, 9(5), 600–613, 2008.
[46] F. Gruttmann, W. Wagner, "Shear correction factors in Timoshenko's beam theory for arbitrary shaped cross-sections", Computational Mechanics, 27, 199–207, 2001.
[47] G.R. Cowper, "The shear coefficient in Timoshenko's beam theory", Journal of Applied Mechanics, 33(2), 335–340, 1966.
[48] C. Bach, R. Baumann, "Elastizität und Festigkeit", Springer, Berlin, 1924.
[49] D. Stojek, "Zur schubverformung in biegebalken", ZAMM, 44, 393–396, 1964.
[50] E. Carrera, S. Brischetto, "Analysis of thickness locking in classical, refined and mixed multilayered plate theories", Composite Structures, 82(4), 549–562, 2008.
[51] E. Carrera, S. Brischetto, "Analysis of thickness locking in classical, refined and mixed theories for layered shells", Composite Structures, 85(1), 83–90, 2008.
[52] K.J. Bathe, " Finite element procedure", Prentice hall, 1996.
[53] S.P. Timoshenko, J.N. Goodier, "Theory of elasticity", McGraw-Hill, 1970.
[54] G. Giunta, F. Biscani, E. Carrera, S. Belouettar, "Analysis of Thin-Walled Beams via a One-Dimensional Unified Formulation", International Journal of Applied Mechanics, Submitted.
[55] G. Giunta, S. Belouettar, E. Carrera, "Analysis of FGM beams by means of a unified formulation", IOP Conference Series: Material Science and Engineering, accepted.

[56] G. Giunta, S. Belouettar, E. Carrera, "Analysis of FGM Beams by means of Classical and Advanced Theories", Mechanics of Advanced Materials and Structures (Special Issue on FGM), accepted.